A PLANETARY PERSPECTIVE OF LIFE

A thesis by

MICHAEL L. WONG

In partial fulfillment of the requirements
for the degree of
Doctor of Philosophy

California Institute of Technology
Pasadena, CA
Graduation Year: 2018
Defended: May 31, 2018

ACKNOWLEDGEMENTS

Thank you to Michele Judd and the rest of the Keck Institute for Space Studies staff for allowing me to use the KISS facilities as the perfect writing hideout.

The rest of you know who you are.

ABSTRACT

In this thesis, I explore the photochemistry of a possible ancient Titan climate state called Snowball Titan, the photochemistry of Pluto during the New Horizons encounter, and the photochemistry of Hadean Earth with implications for the emergence of life. Discussions of the three worlds are divided into three chapters: Chapter 1 is the published work "Pluto's Implications for a Snowball Titan"; Chapter 2 is the published work "The Photochemistry of Pluto's Atmosphere as Illuminated by New Horizons" and the work in progress "Supersaturated Water Vapor as Pluto's Mysterious Atmospheric Coolant"; Chapter 3 is the published work "Nitrogen Oxides in Earth's Early Atmosphere as Electron Acceptors for Life." In all works, we use the Caltech/JPL chemistry–transport model KINETICS to assess the chemical production, loss, and transport in the planetary atmosphere in question. These models are often informed by other models or spacecraft data. In the case of Snowball Titan and early Earth, we also take advantage of general circulation models as inputs for our photochemical model. In the case of Snowball Titan and present-day Pluto, we use spacecraft data from Cassini and New Horizons, respectively, to constrain and analyze our results. The main findings are:

1) The Snowball Titan state precipitates an order of magnitude less material, and, unlike on present-day Titan, most of that is in nitrile form. A long-lived Snowball Titan climate could potentially explain the "missing

hydrocarbon ocean" on Titan and also the composition of Titan's dunes, which we suggest are solid nitriles created during a Snowball Titan epoch.

2) Pluto's C_2-hydrocarbon profiles can be explained by condensation onto fractal aggregate aerosols. Fitting the New Horizons data constrains the sticking coefficients for C_2 hydrocarbons and HCN. H_2O could be a strong cooling agent in Pluto's atmosphere if its sticking coefficient is low enough ($\leq 10^{-5}$) to permit supersaturation by ~10 orders of magnitude.
3) Nitrogen oxides are produced in abundance in early Earth's CO_2–N_2 atmosphere via lightning and photochemistry. HNOx species would rain out in to Earth's early ocean and create micromolar concentrations or higher of NO_3^- and NO_2^-. Once at alkaline hydrothermal vents, nitrate and nitrite could have served as high potential electron acceptors to kickstart the emergence of the first metabolic engine and hence the path to life as we know it.

Finally, in the conclusions, I tie together these works by building a new cosmic context in which to view life on Earth and the possibility of other lifeforms across the cosmos.

PUBLISHED CONTENT

IN CHAPTER I

Wong, M.L. , Yung, Y.L. , Gladstone, G.R. (2015) Pluto's Implications for a Snowball Titan. *Icarus* 246, 192–196. DOI: 10.1016/j.icarus.2014.05.019

M.L.W. participated in the conception of the project, ran the photochemical model, analyzed and plotted the results, and wrote the manuscript

IN CHAPTER II

Wong, M.L., Fan, S., Gao, P., et al. (2017) The Photochemistry of Pluto's Atmosphere as Illuminated by New Horizons. *Icarus* 287, 110–115. DOI: 10.1016/j.icarus.2016.09.028

M.L.W. helped run the photochemical model, analyzed the results, and wrote the manuscript

IN CHAPTER III

Wong, M.L., Charnay, B.D., Gao, P., Yung, Y.L, Russell, M.J. (2017) Nitrogen Oxides in Earth's Early Atmosphere as Electron Acceptors for Life. *Astrobiology* 17, 11, 975–983. DOI: 10.1089/ast.2016.1473

M.L.W. participated in the conception of the project, coordinated with the GCM results, ran the photochemical model, analyzed and plotted the results, and wrote the manuscript

TABLE OF CONTENTS

CHAPTER I

HAZY WITH A CHANCE OF LIFE

Pluto's Implications for a Snowball Titan

MICHAEL L. WONG[1], YUK L. YUNG[1], G. RANDALL GLADSTONE[2]

[1]*Division of Geological and Planetary Sciences, California Institute of Technology, Pasadena, CA 91125, USA*
[2]*Southwest Research Institute, Boulder, CO 80302, USA*

Published in *Icarus*
Vol. 246, pp. 192–196
January 15, 2015

ABSTRACT

The current Cassini–Huygens Mission to the Saturn system provides compelling evidence that the present state of Titan's dense atmosphere is unsustainable over the age of the Solar System. Instead, for most of its existence, Titan's atmosphere might have been in a Snowball state, characterized by a colder surface and a smaller amount of atmospheric CH_4, similar to that of Pluto or Triton. We run a 1-D chemical transport model and show that the rates of organic synthesis on a Snowball Titan are significantly slower than those on present-day Titan. The primary method of methane destruction—photosensitized dissociation in the stratosphere—is greatly dampened on Snowball Titan. The downward flux of higher-order molecules through the troposphere is dominated not by hydrocarbons such as ethane, as is the case on Titan today, but by nitriles. This result presents a testable observation that could confirm the Snowball Titan hypothesis. Because Pluto's atmosphere is similar to Titan's in composition, it serves as a basis for comparison. Future observations of Pluto by the New Horizons Mission will inform photochemical models of Pluto's atmosphere and can help us understand the photochemical nature of paleo-Titan's atmosphere.

1. INTRODUCTION

It is likely that Titan's current atmosphere is transient (Lorenz et al., 1997) and that, surprisingly, we human observers have arrived at a privileged time to witness this evanescent state rupturing the humdrum of Titan's paleoclimate. Evidence for the ephemeral nature of Titan's atmosphere comes from data gathered by the Cassini–Huygens mission (Tobie et al., 2006). Prior to the probe's arrival at Titan, it was believed that vast oceans of methane (CH_4) and higher-order hydrocarbon photoproducts covered the icy moon's surface (Lunine et al., 1983; Yung et al., 1984). This mammoth liquid reservoir would resupply atmospheric methane and be a catchment for hydrocarbon rain over the age of the Solar System. Cassini radar observations have found lakes and seas concentrated in the northern polar region that appear to contain a mixture of methane and ethane. However, at ~3×10^4 km^3 in total volume (Lorenz et al., 2008), or ~36 cm of equivalent global average depth, they are far too small to be the hypothesized buffer reservoir for Titan's gaseous methane or the dregs of billions of years of intense atmospheric photochemistry. The photochemical lifetime of the current amount of methane in Titan's atmosphere is a few 10s of Myr, so it is has been suggested that Titan's atmosphere existed without an abundance of methane for most of geologic time and will return to such a state in the future (Lorenz et al., 1997).

Titan's present methane-rich atmosphere probably comes from a geologically recent outgassing event. The discovery of radiogenic ^{40}Ar—the decay product of ^{40}K, which is contained in the rocky part of Titan's interior—is a

smoking gun for significant outgassing. The $^{15}N/^{14}N$ and $^{13}C/^{12}C$ isotope ratios suggest that the nitrogen inventory has undergone significant escape while the carbon inventory has not, corroborating the claims that Titan's atmospheric nitrogen has been present since the moon's formation and that methane arrived later (Niemann et al., 2005; Tobie et al., 2009). Episodic eruptions of methane are thought to have occurred at certain intervals throughout Titan's ~4.5 Gyr history: first during internal differentiation and silicate core formation, then during the onset of convection in the silicate core, and finally during subsequent cooling and crystallization of the outer layer. In the current/latest outgassing episode, which began ~0.5 Ga, part of the subsurface ammonia-doped water ocean crystallized into an ice I layer underneath a layer of methane clathrate. This ice I layer then became unstable against thermal convection; hot thermal plumes (favored by tidal dissipation) rose into the clathrate layer and induced the dissociation of methane clathrates. Eruptive processes then released this methane into the atmosphere, transforming it into the great factory for organic synthesis that it is today (Tobie et al., 2006).

The present atmosphere is built upon a fragile balance between radiation, chemistry, and dynamics—in other words, it is a house of cards, with methane its foundation. CH_4 is the principal molecule in Titan photochemistry. It all begins when CH_4 is photolyzed in the mesosphere and results in the creation of C_2H_2, which then descends into the stratosphere where it is photolyzed, unleashing the highly reactive radical C_2H. C_2H readily attacks and destroys stratospheric CH_4, completing the process known as *photosensitized dissociation* (Yung et al., 1984).

This expedites the photochemistry that ultimately produces the organic compounds and tholins that compose the distinctive haze of Titan's contemporary atmosphere. The organic aerosols that are generated in the stratosphere absorb solar UV and visible radiation, creating a thermal inversion that inhibits vertical transport of higher hydrocarbons. Thus, there is a positive feedback cycle: the concentration of higher hydrocarbons results in more photosensitized dissociation of CH_4, which amplifies the buildup of complex organic molecules.

Without as much methane, the nature of Titan's atmosphere changes dramatically. The greenhouse effect on Titan is dominated by collisional-induced absorption of N_2-N_2, CH_4-N_2, and H_2-N_2 (McKay et al., 1991). Since methane photolysis drives the production of H_2, a methane-free atmosphere would have nothing but collision-induced absorption of N_2-N_2 to supply the greenhouse effect. Therefore, surface temperatures are bound to be colder. The structure of the atmosphere would be quite different as well. Currently, stratospheric haze absorbs solar radiation, keeping temperatures ~180 K in the lower stratosphere. If this haze were to vanish, temperatures in the stratosphere would fall to ~50 K, and the thermal inversion would disappear (Charnay et al., 2014). Hydrocarbons more easily condense out of a colder atmosphere, stifling photochemistry. We call this state "Snowball Titan," after the Snowball Earth hypothesis. During Earth's several Snowball eras, the planet was characterized by a much colder climate and global glaciation (see, e.g., Kirschvink et al., 2000; Kopp et al., 2005). Only after sufficient release of volcanic CO_2 into the atmosphere did temperatures rise enough to melt

the ice. On Titan, CH_4 is the analogous species that must be outgassed to reverse a global frostbite.

2. MODEL

In this study, we use the Caltech/JPL chemistry-transport model (Yung et al., 1984) to simulate the photochemistry of a Snowball Titan atmosphere with far less gaseous CH_4 than in the current epoch. This one-dimensional model contains 91 altitude levels spanning from the surface to 1500 km. We calculate chemical production and loss rates at each altitude as well as diffusive flux between each altitude grid by solving the 1-D continuity equation:

$$\frac{\partial n_i}{\partial t} + \frac{\partial \phi_i}{\partial z} = P_i - L_i, \quad (1)$$

where n_i is the number density for species i, ϕ_i the vertical flux, P_i the chemical production rate, and L_i the chemical loss rate, all evaluated at time t and altitude z. The vertical flux is given by

$$\phi_i = -\frac{\partial n_i}{\partial z}(D_i + K_{zz}) - n_i\left(\frac{D_i}{H_i} + \frac{K_{zz}}{H_{atm}}\right) - n_i \frac{\partial T}{\partial z}\left[\frac{(1+\alpha_i)D_i + K_{zz}}{T}\right], \quad (2)$$

where D_i is the species' molecular diffusion coefficient, H_i the species' scale height, H_{atm} the atmospheric scale height, α_i the thermal diffusion parameter, K_{zz} the

vertical eddy diffusion coefficient, and T the temperature (Yung and DeMore, 1999).

The paleo-Titan temperature profile is taken from Charnay et al.'s (2014) 3-D Global Climate Model of a pure-nitrogen atmosphere (Fig. 1), and chemical reactions and associated rate coefficients are obtained from Moses et al. (2005), with modifications from Li et al. (2014). We fix the methane mixing ratio near the surface to 1.57×10^{-4}, its saturation mixing ratio at the tropopause of a frigid paleo-Titan. For comparison, the present-day mixing ratio at the surface of Titan is 0.014—two orders of magnitude higher. We allow for escape to space of H and H_2, with escape velocities of 2.5×10^4 cm s^{-1} and 6.1×10^3 cm s^{-1}, respectively (Yung et al., 1984). All other species are assumed to be gravitationally bound to Titan.

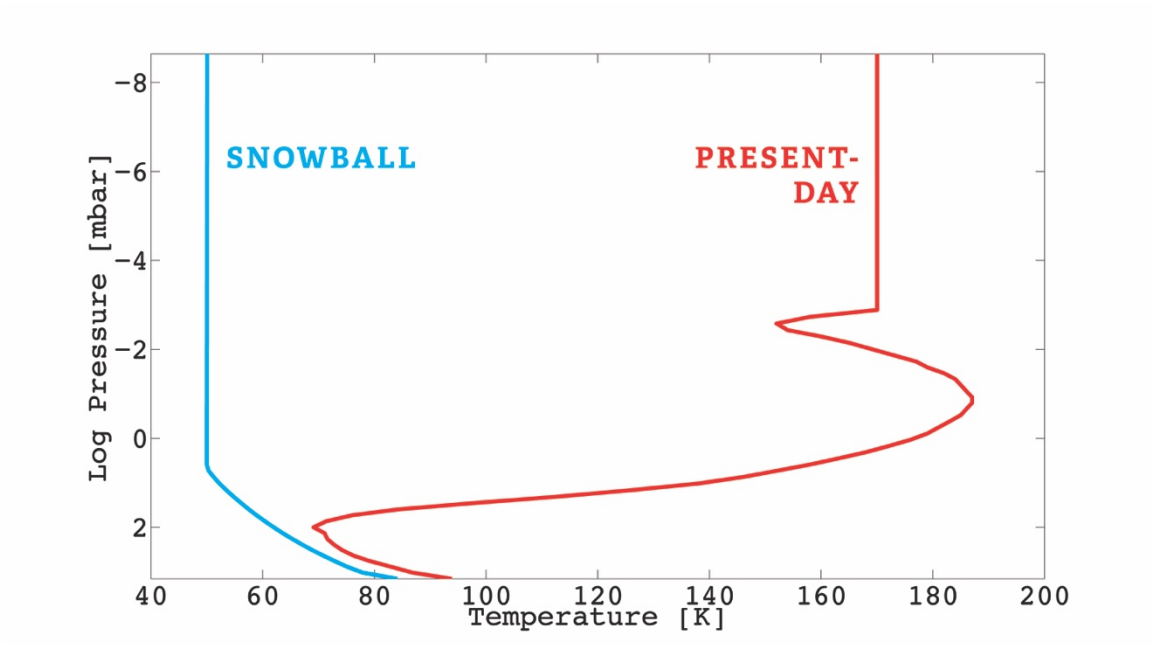

Figure 1. In blue: the temperature profile for Snowball Titan, from Charnay et al. (2013). In red, dashed: the temperature profile used in our present-day Titan model. Note that the thermal inversion around 100 mbar that plays a critical role in the photochemical production on present-day Titan is absent in the Snowball Titan temperature profile.

For both the Snowball and present-day models, we use the current solar luminosity. Although stellar models describe a "faint young Sun" with as little as 70% of its total present output, the UV emissions relevant for hydrocarbon dissociation were actually stronger in the past. We ran a test case raising the energy flux for radiation between 1–1180 Å by a factor of four, corresponding to a ~1.5-Gyr-old Sun (Ribas et al., 2005). The downward fluxes of photochemical products in our model changed by less than 10%. Thus, we conclude that our Snowball Titan results are applicable over a wide range of geologic history.

3. RESULTS

3.1 HYDROCARBON PROPORTIONS

We run photochemical models to simulate both paleo-Titan's and present-day Titan's atmospheres. In Fig. 2, we show a comparison between the mixing ratio profiles for CH_4 and the three major C_2 photoproducts for Snowball Titan and current Titan. While the present-day Titan model has been laboriously fine-tuned to fit measurements from Cassini (Krasnopolsky, 2009; Li et al., 2014; Wilson and Atreya, 2009; Yung et al., 1984), the major hydrocarbon mixing ratios are reduced by 2–3 orders of magnitude on Snowball Titan.

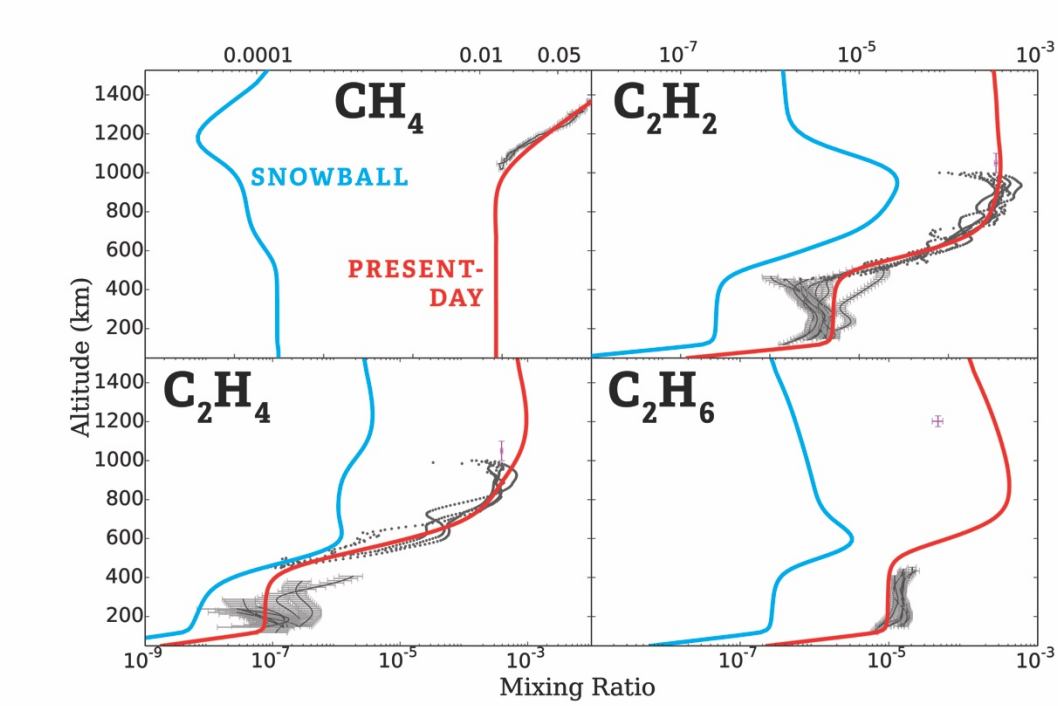

Figure 2. Comparison between Snowball Titan and present-day Titan. Underplotted in gray are the Cassini data (Magee et al. 2009, Kammer et al. 2010, Koskinen et al. 2010, Vinatier et al. 2010, Westlake et al. 2011).

A quantity of great interest is the downward flux of photoproducts on paleo-Titan, especially that of ethane (C_2H_6). Table 1 compares the fluxes at the base of the tropopause from the two models. Modern Titan has a downward ethane flux at the tropopause of ~3×10^9 molecules cm^{-2} s^{-1}; over ~4 Gyr, this would generate a global ocean of liquid ethane hundreds of meters deep. Our calculations show that on paleo-Titan, the downward ethane flux at the tropopause is reduced to ~8×10^7 molecules cm^{-2} s^{-1}, which produces only a ~2 m global layer of ethane over Titan's history. Although this is still a significant body of liquid that no longer exists on Titan's surface, it is much more plausible that it could almost entirely be removed (via absorption into porous regolith and/or in the form of clathrate hydrates, for instance) and result in the ~36 cm globally averaged layer of liquid we observe on

Titan. Thus, the absence of a deep global ocean of hydrocarbons is consistent with the supposition that Titan existed in a Snowball state throughout most of its history.

Species	Present-day Titan flux [cm^{-2} s^{-1}]	Fraction of C mass flux	Snowball Titan flux [cm^{-2} s^{-1}]	Fraction of C mass flux
CH_4	1.07×10^{10}	–	1.30×10^{9}	–
C_2H_2	-1.50×10^{9}	2.97×10^{-1}	-7.34×10^{7}	1.10×10^{-1}
C_2H_4	-2.30×10^{7}	4.54×10^{-3}	-1.59×10^{6}	2.38×10^{-3}
C_2H_6	-2.89×10^{9}	5.72×10^{-1}	-7.84×10^{7}	1.17×10^{-1}
C_3H_8	-1.22×10^{8}	3.62×10^{-2}	-1.42×10^{5}	3.19×10^{-4}
CH_3C_2H	-5.47×10^{6}	1.62×10^{-3}	-7.56×10^{6}	1.70×10^{-2}
Total downward flux of C atoms from hydrocarbons	-9.22×10^{9}	9.12×10^{-1}	-3.30×10^{8}	2.47×10^{-1}
HCN	-5.37×10^{8}	5.30×10^{-2}	-3.75×10^{8}	2.81×10^{-1}
HC_3N	-9.71×10^{6}	2.88×10^{-3}	-3.10×10^{5}	6.97×10^{-4}
C_2H_3CN	-7.26×10^{7}	2.15×10^{-2}	-5.89×10^{7}	1.32×10^{-1}
C_2N_2	-5.45×10^{5}	1.08×10^{-4}	-2.07×10^{6}	3.10×10^{-3}
HC_5N	-1.85×10^{6}	9.13×10^{-4}	-5.61×10^{6}	2.10×10^{-2}
C_6N_2	-1.66×10^{7}	9.82×10^{-3}	-7.02×10^{7}	3.15×10^{-1}
Total downward flux of C atoms from nitriles	-8.93×10^{8}	8.83×10^{-2}	-1.01×10^{9}	7.53×10^{-1}
Total downward flux of C atoms	-1.01×10^{10}	–	-1.34×10^{9}	–

Table 1. Fluxes at the tropopause for present-day and Snowball Titan; positive flux is upward.

On Titan today, the ethane production is nearly double that of acetylene (C_2H_2). On Snowball Titan, we predict that the downward fluxes of these two

hydrocarbons would have been roughly similar. Therefore, there should exist an inventory of acetylene on the surface of Titan comparable in size to the ~2 m global equivalent layer of ethane. Titan's surface is cold enough for acetylene to freeze, so solid acetylene could be held as sedimentary material in Titan's crust and/or a major constituent of Titan's dunes. Indeed, the estimated dune volume of a few × 10^5 km^3 (Le Gall et al., 2012) is a sufficient reservoir for the acetylene generated by Snowball Titan over geologic time. This result helps explain a major puzzle regarding Titan's organic surface reservoirs. It is difficult to explain why Titan's dune volume is an order of magnitude larger than its lake volume using photochemical models of present-day Titan, since they show that the ethane flux is at least twice that of solids such as acetylene. However, our model demonstrates that if Titan existed in a Snowball state throughout most of its history, then the ratio between liquid ethane and solid hydrocarbons on Titan's surface could resemble what we observe today.

3.2 NITRILE DOMINATION

It is convenient to divide the photochemistry of Titan's atmosphere into two regions, characterized by primary and photosensitized processes, respectively. In the thermosphere and mesosphere, dissociation of N_2 and CH_4 occurs by direct photolysis or electron impact. This leads to the production of important species such as C_2H_2, which are transported downward to the lower stratosphere. Here C_2H_2 can drive additional stratospheric chemistry by catalyzing the further dissociation of CH_4. It has been shown that the photosensitized destruction of CH_4

in the stratosphere is primarily responsible for producing the large flux of C_2H_6 on present-day Titan (see, e.g., Li et al., 2014; Yung et al., 1984). On Snowball Titan, the photochemistry driven by primary photolysis of CH_4 is similar to that of the present-day atmosphere. However, the photosensitized dissociation of CH_4 is greatly reduced.

Under Snowball conditions, the hydrocarbon radical concentrations in the stratosphere are curtailed, so that reactions leading to the production of C_2 hydrocarbons, such as

$$CH_2 + CH_2 \longrightarrow C_2H_2 + H_2$$

$$CH_2 + CH_3 \longrightarrow C_2H_4 + H$$

must compete with reactions such as

$$N + CH_2 \longrightarrow HCN + H$$

$$N + CH_3 \longrightarrow HCN + H_2.$$

The latter reactions result in the enhanced production of HCN and eventually other nitrile compounds.

Indeed, on Snowball Titan, most of the downward mass flux of carbon at the tropopause is due to the descent not of hydrocarbons but of nitriles. Our model predicts that, by mass, nitriles compose 75 percent of the downward carbon flux in the Snowball state. In contrast, this quantity is less than 9 percent for contemporary Titan. Put differently, Titan as we know it is Nature's great hydrocarbon factory, but Titan of the past (and possibly the future) was Nature's great nitrile factory. Since the total downward flux of photoproducts is an order of magnitude greater

on contemporary Titan, both present-day and Snowball Titan have a global nitrile deposition rate of ~10^{-5} m kyr^{-1}. Fig. 3 summarizes the comparison between the proportion of hydrocarbon and nitrile fluxes in each state.

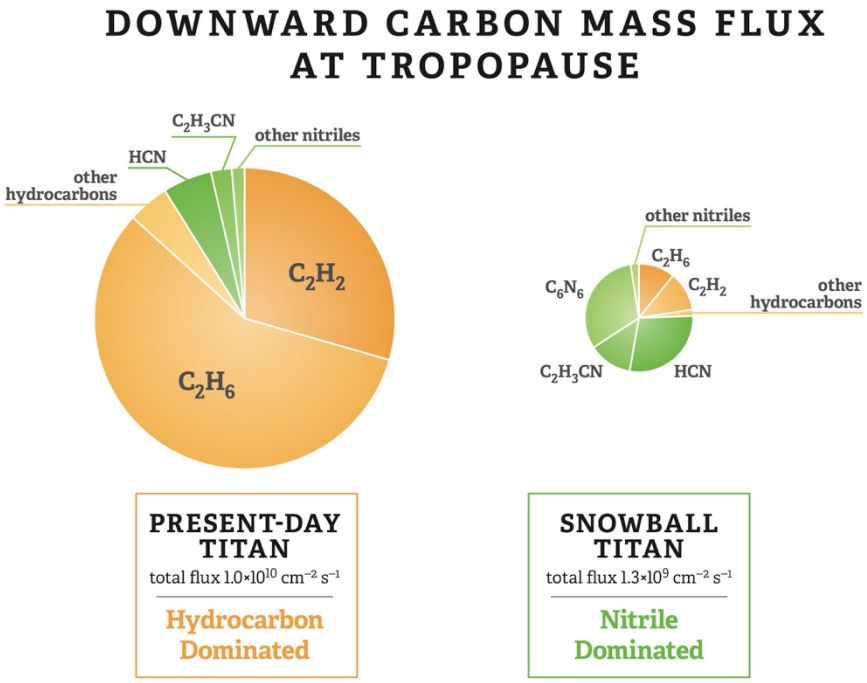

Figure 3. These pie charts show the relative contributions to the carbon mass flux at the tropopause for present-day Titan and Snowball Titan. Carbon mass flux can be thought of as a measure of the ultimate "fate" of a methane carbon atom, which is liberated from its tetrahedral cage via photolysis, and eventually partners with other C atoms (forming higher-order hydrocarbons) or N atoms (forming nitriles).

The area of a slice is proportional to the downward carbon mass flux that a certain species carries. The flux per area is equal in both charts, so the total area of the Snowball Titan pie is 0.13 that of present-day Titan.

On present-day Titan, hydrocarbons make up over 90 percent of the carbon mass flux, with C_2H_6 the major contributor. On Snowball Titan, the carbon mass flux is dominated by nitriles, and C_2H_6 and C_2H_2 contribute equally to the downward hydrocarbon flux. The total carbon mass flux for Snowball Titan is an order of magnitude less than that of present-day Titan.

Simple sensitivity studies show that increasing the stratospheric temperature by 10s of K does not alter nitrile domination over hydrocarbons on Snowball Titan. Above ~100 km, the concentration of N is still much greater than CH_3 or CH_2, resulting in the preferred creation of HCN and other nitriles through the second pair of chemical reactions above. Indeed, with increasing stratospheric temperature, the downward flux of nitriles grows while the downward flux of hydrocarbons decreases. For instance, changing stratospheric temperature to ~170 K reduces the C_2H_6 flux by a factor of 3 while increasing the HCN flux by ~30 percent.

4. DISCUSSION & CONCLUSIONS

Although the photochemistry of paleo-Titan likely bears little resemblance to that of present-day Titan, it may be related to that of Pluto. As a cold dwarf planet with a tenuous nitrogen-dominated atmosphere, Pluto provides a guideline for the photochemistry on Snowball Titan, especially on the suppression of photosensitized dissociation of CH_4. This distant Kuiper belt world also serves as a case study for the relative importance of the formation of higher hydrocarbons versus nitriles. Furthermore, Pluto is a test bed for global warming and cooling, particularly for the impact of such changes on the condensation of N_2 and CH_4 as solar forcing varies seasonally. Finally, Pluto gives us a gauge for the eddy diffusion and planetary boundary layer structure on Snowball Titan.

Krasnopolsky and Cruikshank (1999) modeled the photochemistry of Pluto's atmosphere. They found that on Pluto, the acetylene precipitation is nearly tenfold that of ethane. The leading nitrile precipitant is HC_3N; its downward molecular flux is greater than ethane's by a factor of a few. Although Krasnopolsky and Cruikshank predict that hydrocarbons are the primary precipitant in Pluto's atmosphere (thanks to acetylene's great contribution), nitriles do account for a pronounced fraction of the downward carbon flux.

Photosensitized dissociation is the most effective method of methane destruction on present-day Titan. However, its importance is greatly reduced on Pluto due to competing reactions of C_2H with other hydrocarbons. Some of these reactions regenerate C_2H_2 (Krasnopolsky and Cruikshank, 1999). Similarly, photosensitized dissociation on Snowball Titan is dampened, but for a different reason. Since Snowball Titan still contains a dense nitrogen atmosphere, the dissociation of N_2 (by both photolysis *and* plasma reaction due to Saturn's magnetosphere) leads to a prevalence of N that reacts with CH_2 and CH_3 to form nitriles instead of C_2H_2. Thus, the precipitants on each world (acetylene domination on Pluto, nitrile domination on Snowball Titan) are directly linked to the respective causes of their reduced photosensitized dissociation.

If Titan existed in the Snowball state explored in this study, the satellite's surface should contain a larger deposit of nitriles than hydrocarbons. Recall that according to our models, the total amount of nitrile deposition is the similar in both the present-day and Snowball cases; thus, it is imperative to compare the proportion of nitriles to hydrocarbons on the surface of Titan to discern which state dominated

the satellite's history. The discovery of more nitrile material by future orbiters/landers would be a significant validation of the Snowball Titan theory.

It is also possible that Titan's past atmospheric temperature profile was even colder than the one used in our model; consequently, large amounts of nitrogen would condense onto the surface, thinning the atmosphere. In this case, Snowball Titan might resemble Pluto even more. If ensuing missions discover that Titan's surface inventory of acetylene vastly outweighs its nitrile sediment, then this could point to an ancient Titan atmosphere significantly depleted in nitrogen as well as methane.

Since New Horizon's encounter at Pluto will provide an assessment of the Pluto photochemistry models, which in turn aid us in describing possible scenarios for Titan's past and future, we are looking forward to the New Horizons Mission with great interest.

ACKNOWLEDGEMENTS

This research was supported in part by the Cassini UVIS program via NASA grant JPL.1459109, NASA NNX09AB72G grant to the California Institute of Technology. YLY was supported in part by the New Horizons mission. We thank J. Kammer, C. Li, P. Gao, P. Kopparla, X. Zhang, D. Piskorz, and H. Ngo for helpful comments. Special thanks are due to C. Sotin for making available his model prior to publication. We are grateful for the comments and suggestions from our two anonymous reviewers.

CHAPTER II

THE DEVIL IN THE DARK

The Photochemistry of Pluto's Atmosphere as Illuminated by New Horizons

MICHAEL L. WONG[1], SITENG FAN[1], PETER GAO[1], MAO-CHANG LIANG[2], RUN-LIE SHIA[1], YUK L. YUNG[1], JOSHUA A. KAMMER[3], MICHAEL E. SUMMERS[4], G. RANDALL GLADSTONE[5,6], LESLIE A. YOUNG[3], CATHERINE B. OLKIN[3], KIMBERLY ENNICO[7], HAROLD A. WEAVER[8], S. ALAN STERN[3], AND THE NEW HORIZONS SCIENCE TEAM

[1]*Division of Geological and Planetary Sciences, California Institute of Technology, Pasadena, CA 91125, USA*
[2]*Research Center for Environmental Changes, Academia Sinica, Taipei 115, Taiwan*
[3]*Southwest Research Institute, Boulder, CO 80302, USA*
[4]*George Mason University, Fairfax, VA 22030, USA*
[5]*Southwest Research Institute, San Antonio, TX 78238, USA*
[6]*University of Texas at San Antonio, San Antonio, TX 78249, USA*
[7]*National Aeronautics and Space Administration, Ames Research Center, Space Science Division, Moffett Field, CA 94035, USA*
[8]*The Johns Hopkins University Applied Physics Laboratory, Laurel, MD 20723, USA*

Published in *Icarus*
Vol. 287, pp. 110–115
May 1, 2017

ABSTRACT

New Horizons has granted us an unprecedented glimpse at the structure and composition of Pluto's atmosphere, which is comprised mostly of N_2 with trace amounts of CH_4, CO, and the photochemical products thereof. Through photochemistry, higher-order hydrocarbons are generated, coagulating into aerosols and resulting in global haze layers. Here we present a state-of-the-art photochemical model for Pluto's atmosphere to explain the abundance profiles of CH_4, C_2H_2, C_2H_4, and C_2H_6, the total column density of HCN, and to predict the abundance profiles of oxygen-bearing species. The CH_4 profile can be best matched by taking a constant-with-altitude eddy diffusion coefficient K_{zz} profile of 1×10^3 cm^2 s^{-1} and a fixed CH_4 surface mixing ratio of 4×10^{-3}. Condensation is key to fitting the C_2 hydrocarbon profiles. We find that C_2H_4 must have a much lower saturation vapor pressure than predicted by extrapolations of laboratory measurements to Pluto temperatures. We also find best-fit values for the sticking coefficients of C_2H_2, C_2H_4, C_2H_6, and HCN. The top three precipitating species are C_2H_2, C_2H_4, and C_2H_6, with precipitation rates of 179, 95, and 62 g cm^{-2} s^{-1}, respectively.

1. INTRODUCTION

In July 2015, New Horizons performed its historic flyby of Pluto, giving humanity an unprecedented view of the dwarf planet's atmosphere. One of New Horizons' goals was to determine the structure, composition, and variability of Pluto's atmosphere. The Alice instrument measured the full disk spectral flux in ultraviolet wavelengths between 52 and 187 nm as the Sun slid behind Pluto (ingress) and emerged on the other side (egress), about one hour after closest approach. This observation has been used to determine the temperature and vertical density profiles of N_2, CH_4, and various minor species in Pluto's atmosphere. Nearly simultaneous Earth ingress and egress occultations, observed in the X-band uplink, provided profiles of temperature and pressure in Pluto's lower atmosphere (Gladstone et al., 2016).

Thanks to New Horizons, Pluto's basic atmospheric composition—at least at the time of the encounter—is now known. The task now falls to the modelers to explain Pluto's atmosphere, which defied expectations on multiple accounts. For instance, Pluto's atmosphere is far colder than anticipated. It has been suggested that this is due to radiative cooling by HCN (Gladstone et al., 2016). Despite its colder nature, Pluto seems to still produce photochemical hydrocarbons and nitriles—whose abundance profiles have been measured—to a significant degree. The most striking product of this photochemical factory is the extensive haze layers that New Horizons confirmed via optical images (Gladstone et al., 2016). A

companion paper in this issue (Gao et al., 2016) investigates the microphysics behind haze production on Pluto.

The central goal of this study is to reproduce New Horizons' observations of CH_4, the C_2 hydrocarbons, as well as to predict abundances other trace species that have not yet been detected with as much precision. The New Horizons data gives reliable measurements for CH_4 above 200 km and C_2 hydrocarbons between 800 and 200 km. Above 800 km, the signal-to-noise is too small to retrieve trace species' abundances. Below ~200, the measurements are no longer sensitive to CH_4, because all the photons shortward of 140 nm are gone, and this causes an artifact in the retrieval algorithm that makes the C_2H_6 detection nonphysical and the C_2H_2 detection untrustworthy. However, thanks to its strong, unique spectral features, C_2H_4 abundances are robust from 800 km to the surface.

2. PHOTOCHEMICAL MODEL

We use the one-dimensional Caltech/JPL chemistry-transport model KINETICS (Allen et al., 1981; Yung and DeMore, 1999) to explore the nature of Pluto's atmosphere. Because Pluto's atmospheric extent surpasses its solid body radius (r_0 = 1187 km), the atmosphere must be considered spherical (Krasnopolsky and Cruikshank, 1999). The model contains 40 levels ranging from the surface to ~1300 km. Our calculations incorporate 88 chemical species and over 1600 reactions (Li et al., 2015; Yung et al., 1984). We simulate the production and loss rates of trace compounds such as hydrocarbons and nitriles at each altitude, as well as their

diffusive flux between altitude grids, by solving the 1-D continuity equation for a spherical atmosphere:

$$\frac{\partial n_i}{\partial t} + \frac{1}{r^2}\frac{\partial (r^2 \phi_i)}{\partial r} = P_i - L_i, \quad (1)$$

where n_i is the number density for species i, ϕ_i the vertical flux, P_i the chemical production rate, and L_i the chemical loss rate, all evaluated at time t and radius $r = r_0 + z$ (where z is the altitude above the surface). The vertical flux is given by

$$\varphi_i = -\frac{\partial n_i}{\partial r}(D_i + K_{zz}) - n_i\left(\frac{D_i}{H_i} + \frac{K_{zz}}{H_{atm}}\right) - n_i \frac{\partial T}{\partial r}\left[\frac{(1+\alpha_i)D_i + K_{zz}}{T}\right], \quad (2)$$

where D_i is the species' molecular diffusion coefficient, H_i the species' scale height, H_{atm} the atmospheric scale height, α_i the thermal diffusion parameter, K_{zz} the vertical eddy diffusion coefficient, and T the temperature (Yung and DeMore, 1999).

The starting ingredients for a photochemical model are the pressure and temperature profiles of the atmosphere. For this study, we use the state-of-the-art profiles retrieved from radio occultation data recorded by New Horizons (Gladstone et al., 2016). These are presented as temperature and total density in Fig. 1.

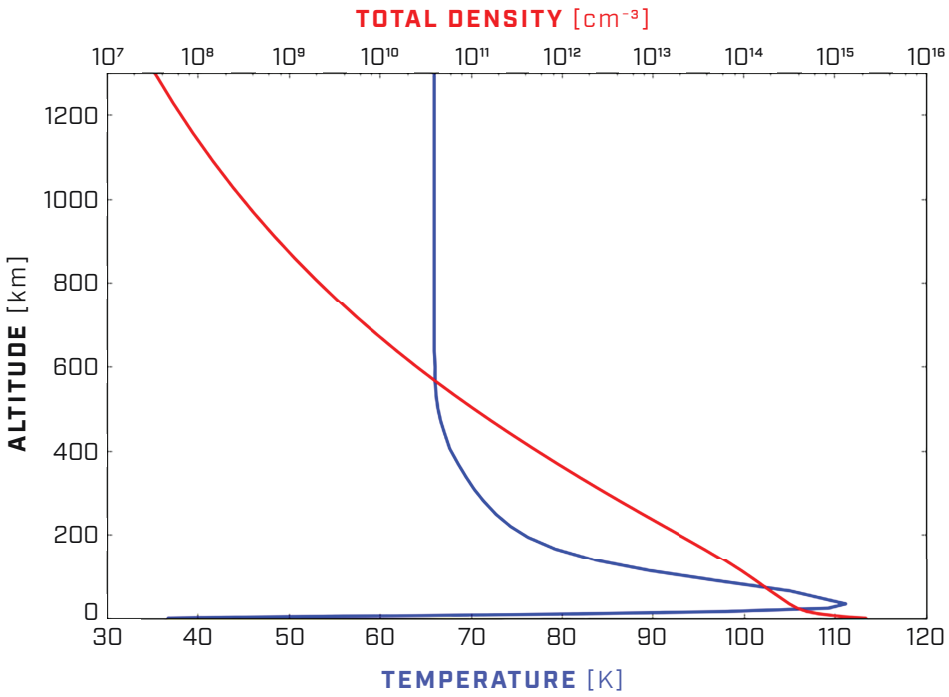

Fig. 1. The temperature and density profiles of Pluto's atmosphere, as determined by data from New Horizons.

Photochemistry is primarily driven by radiation from the Sun. However, the contribution from solar Lyman α scattered from H atoms in the local interstellar medium is known to be significant in the outer Solar System (see, e.g., Moses, Allen, and Yung 1992). We adopt an enhancement factor of 1.43 based on the observations of Gladstone et al. (2015) for our photochemical model. We expect the production rates of hydrocarbons to scale with this factor, as the primary consequence of the destruction of CH_4 is the production of hydrocarbons, followed by condensation.

CH_4 and N_2 are processed by far-ultraviolet and extreme-ultraviolet radiation, respectively, into higher-order hydrocarbons and nitriles. These photochemical products can themselves become photolyzed and interact with each

other to form even more massive species. Many of these reactions are familiar and well understood, as the atmospheric chemistry of Pluto greatly resembles that of Titan (see, e.g., Wong et al., 2015).

However, photochemistry alone cannot explain trace species' overall abundances or the structure of their vertical profiles. It is clear that condensation plays an important role on Pluto.

In the New Horizons data, the major C_2 hydrocarbons increase in abundance towards the surface, but that increase is curtailed somewhere between 400 and 200 km. In a photochemical model that ignores condensation, all C_2 hydrocarbons will increase in abundance all the way to the surface, in contradiction to the data.

Saturation vapor pressures, extrapolated from laboratory measurements to Pluto temperatures, were used as a first guess to predict the condensation of various chemical species (Lara et al., 1996) (Fig. 2a). Pre-formed aerosols would serve as condensation sites. The rate coefficient for a condensable species to be removed by collision with aerosols is given by the formalism of Willacy, Allen, and Yung (2016),

$$J = \frac{1}{4}\gamma v A N \ , \qquad (3)$$

where γ is the sticking coefficient (the fraction of collisions that result in a molecule condensing upon the surface of an aerosol), v is the thermal velocity (cm s^{-1}) of the

molecule, A is the surface area of an aerosol particle (cm^2), and N is the number density of aerosol particles (cm^{-3}). Based on a combination of observations and modeling, Gao et al. (this issue) estimate AN, the mean aerosol surface area per unit volume of atmosphere (Fig. 2b). A priori, J is highly uncertain, and we test a large range of γ to explore its impact on the condensable species.

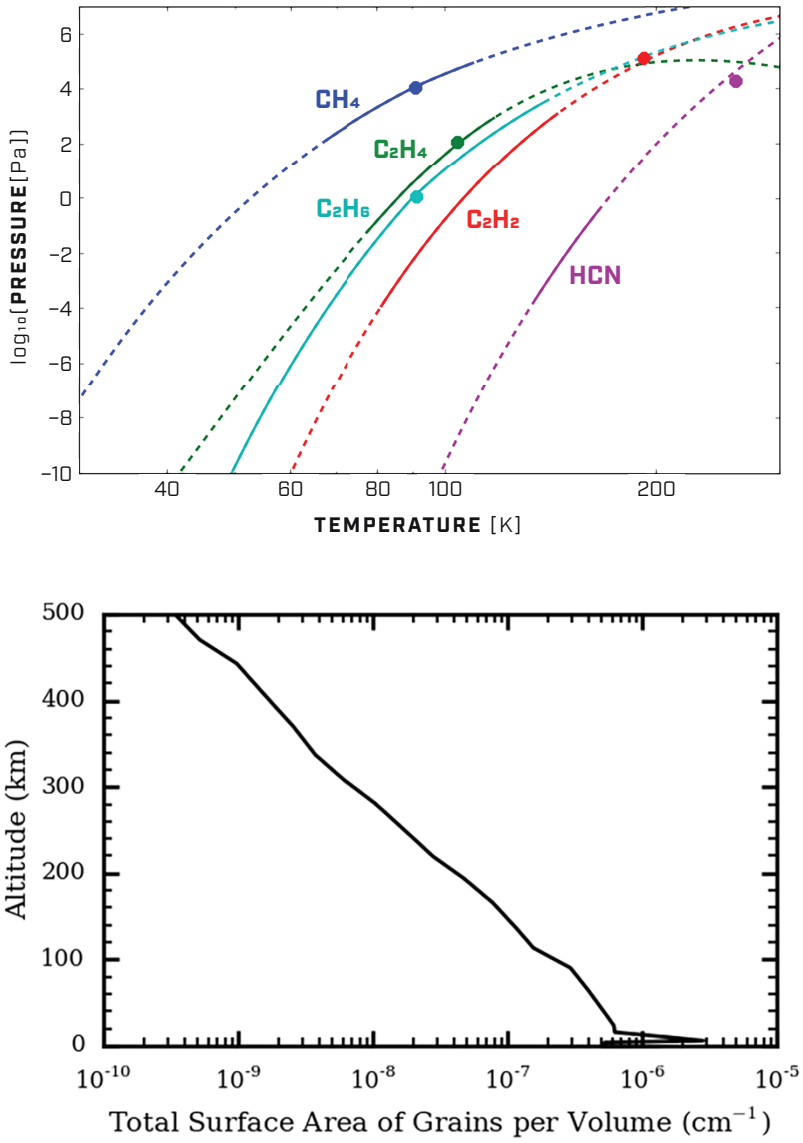

Fig. 2 (a) Saturation vapor pressure curves for various constituents of Pluto's atmosphere. Solid lines represent laboratory measurements. Dashed lines represent extrapolations. Circles indicate the triple points. **(b)** Total surface area of aerosols per volume of atmosphere, as calculated in our companion paper (Gao et al., 2016).

Influx of exogenous material and escape from the top of atmosphere are the final processes that can influence the abundances of chemical species. We incorporate a downward flux of water molecules taken from Poppe (2015), which calculated the influx of interplanetary dust into Pluto's atmosphere as a function of Pluto's location in its orbit within the Kuiper Belt. New Horizons' arrival coincides with a dust flux of 1.4×10^{-17} g cm^{-2} s^{-1}. For simplicity we assume that this entire mass is composed of water ice and is vaporized within Pluto's atmosphere upon infall, thereby giving a downward H_2O flux at the top of the atmosphere of ~5×10^5 molecules cm^{-2} s^{-1}. In terms of loss to space, we assume all species besides H and H_2 are gravitationally bound to Pluto; we allow H and H_2 to escape at their respective Jeans escape velocities.

3. RESULTS

3.1 CH_4

The first dataset we seek to fit is the methane abundance profile. CH_4 is the second most abundant constituent in Pluto's atmosphere and is resupplied by a large solid reservoir on the surface. Direct photolysis is the main mechanism for its loss. As the parent molecule of photochemistry, CH_4 is relatively unaffected by the abundances of higher-order hydrocarbons, which we refine later (Section 3.2). Because CH_4 has a relatively long chemical lifetime, it is sensitive to transport processes. Hence, the CH_4 profile gives us information about the eddy diffusion in Pluto's atmosphere.

To fit the CH_4 profile, we varied two parameters: 1) the K_{zz} profile; 2) the CH_4 mixing ratio at the surface, which we held constant during model runs. Because an analytical expression for the eddy diffusion profile of a tenuous atmosphere like Pluto's has yet to be formulated from first principles, we tested a wide range of K_{zz} profiles by varying the parameter a between 0 and 1.8 in the following simple equation:

$$K_{zz} = 1000 \left(\frac{n_0}{n}\right)^a, \quad (4)$$

where n is the total number density and n_0 is the total number density at the surface. We varied CH_4 surface mixing ratios between 1×10^{-3} to 8×10^{-3}.

Changing the K_{zz} profile essentially changes the *curvature* of the methane profile that the model converges to. High values of a, which correspond to K_{zz} profiles that increase rapidly with altitude, produces flatter CH_4 profiles, because the methane in the upper atmosphere is being transported downwards. On the other hand, when $a = 0$, the K_{zz} profile is constant with altitude, and more CH_4 can exist in the upper atmosphere. To first order, changing the CH_4 surface mixing ratio simply serves as a translation of the CH_4 profile in mixing ratio–altitude space.

We found that a CH_4 surface mixing ratio of 4×10^{-3} and a constant-with-altitude K_{zz} of 1×10^3 cm^2 s^{-1} satisfies the New Horizons data the best. With this K_{zz} profile, the homopause is at Pluto's surface, meaning that molecular diffusion plays an important role throughout Pluto's atmosphere.

3.2 C_2 HYDROCARBONS

With the CH_4 profile established and a plausible K_{zz} profile defined, we now turn to fitting the profiles of the C_2 hydrocarbons. The New Horizons data show that the concentrations of the C_2 hydrocarbons do not monotonically increase towards the surface of Pluto. Instead, they exhibit inversions between 200 and 400 km, most notably in the cases of C_2H_4 and C_2H_2. We attribute these inversions to heterogeneous nucleation: in this region of Pluto's atmosphere, the combination of low temperature and high aerosol surface area makes condensation on hydrocarbon/nitrile aerosols to be the dominant means of removal. The formation and distribution of these aerosols is discussed in Gao et al. (this issue). Above 400 km, there are too few nucleation sites for condensation to be important, and below 200 km, the temperature is too high to allow condensation. Compared to the rate of heterogeneous nucleation, the rate of homogeneous nucleation is far too low for it to be a relevant process at these temperatures and concentrations.

A breakdown of the production and loss mechanisms for C_2H_2, C_2H_4, and C_2H_6 is presented in Fig. 3. Condensation, shown in black, clearly dominates the region between 200 and 400 km.

Using saturation vapor pressure curves extrapolated to Pluto temperatures results in a condensation-induced inversion of the C_2H_2 profile but not the C_2H_4 profile. Fig. 2b illustrates why: at the relevant temperature of ~70 K, the extrapolated saturation vapor pressure of C_2H_4 is several orders of magnitude greater than that of C_2H_2. Based on the evidence provided at Pluto, we conclude

that such an extrapolation of C_2H_4's saturation vapor pressure is inappropriate and that C_2H_4 should behave similarly to C_2H_2 at low temperatures. Thus, we use C_2H_2's saturation vapor pressure curve for both C_2H_2 and C_2H_4, which produces inversions in both species' concentration profiles in our model.

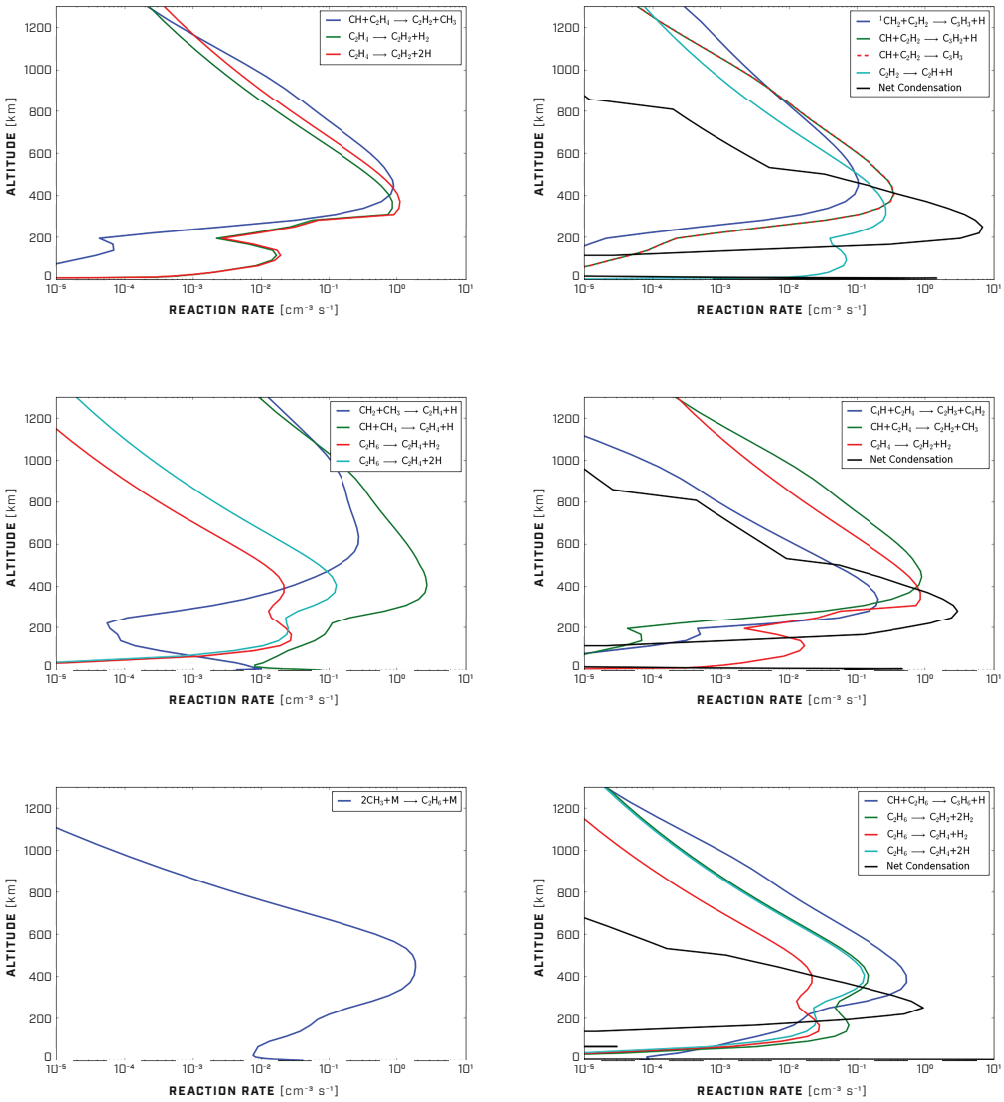

Fig. 3. A breakdown of the mechanisms for production and loss of the major C_2 hydrocarbons at each altitude in Pluto's atmosphere. C_2H_2 production **(a)** and loss **(b)**. C_2H_4 production **(c)** and loss **(d)**. C_2H_6 production **(e)** and loss **(f)**. Between 200 and 400 km, condensation (black) is clearly the dominant loss mechanism for C_2H_2 and C_2H_4, resulting in the inversions in their abundance profiles.

The need to adjust C_2H_4's extrapolated saturation vapor pressure is not evident from photochemical studies of Titan, where C_2H_4 condenses at temperatures >80 K (see Fig. 1 of Lavvas et al., 2011), a temperature range for which we have experimental data (Fig. 2a). New Horizons at Pluto probes the hydrocarbon chemistry of a previously unexplored temperature and pressure space.

Early model runs resulted in condensation that was too strong: photochemical production could not compete with condensation, and our concentrations of C_2H_2 and C_2H_4 underestimated the data by up to a factor of 10. We altered the sticking coefficient γ of each individual species to fit their respective abundance profiles. The sticking coefficient is the fraction of collisions that result in a molecule condensing upon the surface of an aerosol. We found best-fit sticking coefficients of $\gamma_{C2H2} = 3 \times 10^{-5}$, $\gamma_{C2H4} = 1 \times 10^{-4}$, and $\gamma_{C2H6} = 3 \times 10^{-6}$.

By updating the saturation vapor pressures and introducing variable sticking coefficients, we were able to reproduce the general structure of the C_2 hydrocarbon concentration profiles in Pluto's atmosphere (Fig. 4).

Although the parameters we tuned to fit the CH_4 and C_2 hydrocarbon profiles are related in that they all influence the removal of molecules from the atmosphere, they were tuned in a logical, sequential order. The K_{zz} profile has a far greater influence on CH_4 than the other hydrocarbons due to CH_4's long chemical lifetime, and since CH_4 is the parent molecule of all photochemical products, it was prudent to adjust the K_{zz} profile to fit the CH_4 profile first. The concentration profiles of C_2H_2 and C_2H_4 exhibit a condensation-induced inversion between 400

and 200 km; unless C_2H_4's saturation vapor pressure was lower than its extrapolated value at ~70 K, this profile shape could not be achieved. Finally, we tweaked the sticking coefficients of the C_2 species to fit the data more exactly. This systematic tuning reproduced distinct features of Pluto's atmosphere at each step. Varying the K_{zz} in a sensible manner, for instance, could not result in the C_2H_4 inversion shape. Similarly, changing the sticking coefficients could not result in the C_2H_4 inversion shape or help with fitting the CH_4 profile.

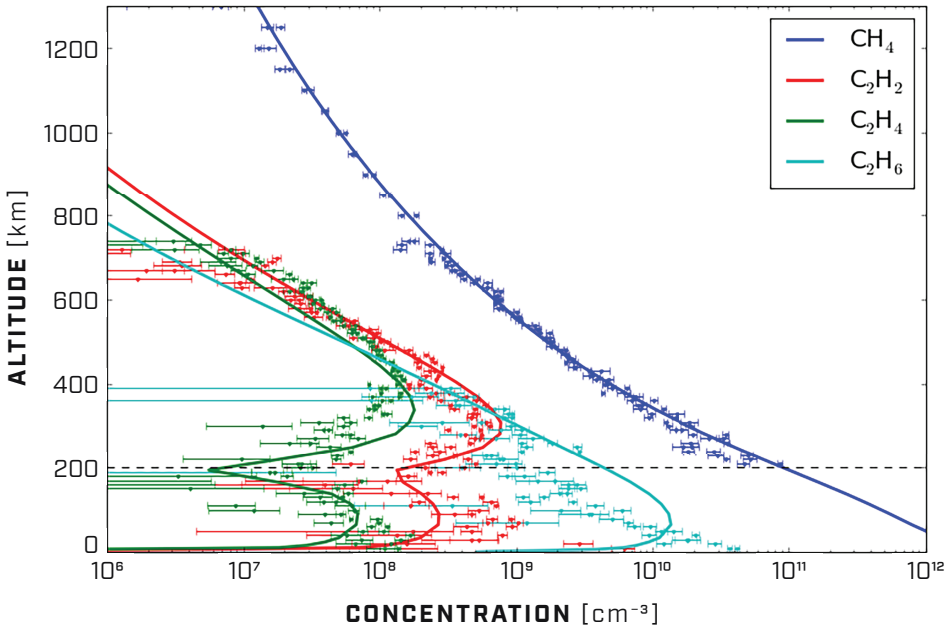

Figure 4. Best-fit model results for CH_4 and the major C_2 hydrocarbons. The data are from Gladstone et al. 2016, Fig. 2c.

3.3 HCN

While New Horizons has not provided detailed constraints on the abundance profile of HCN, ALMA data determined an HCN column density of 5×10^{13}

molecules cm^{-2} (Lellouch et al. 2015). Using an HCN saturation vapor pressure curve extrapolated to Pluto temperatures, we vary the sticking coefficient γ_{HCN} and produce various concentration profiles, each with their own column densities (Fig. 5). We find that $\gamma_{HCN} = 1 \times 10^{-2}$ produces an HCN profile that matches the column density from ALMA observations. That γ_{HCN} is greater than the sticking coefficient of the major C_2 hydrocarbons is consistent with physical intuition: species with larger molecular polarity should be more amenable to sticking.

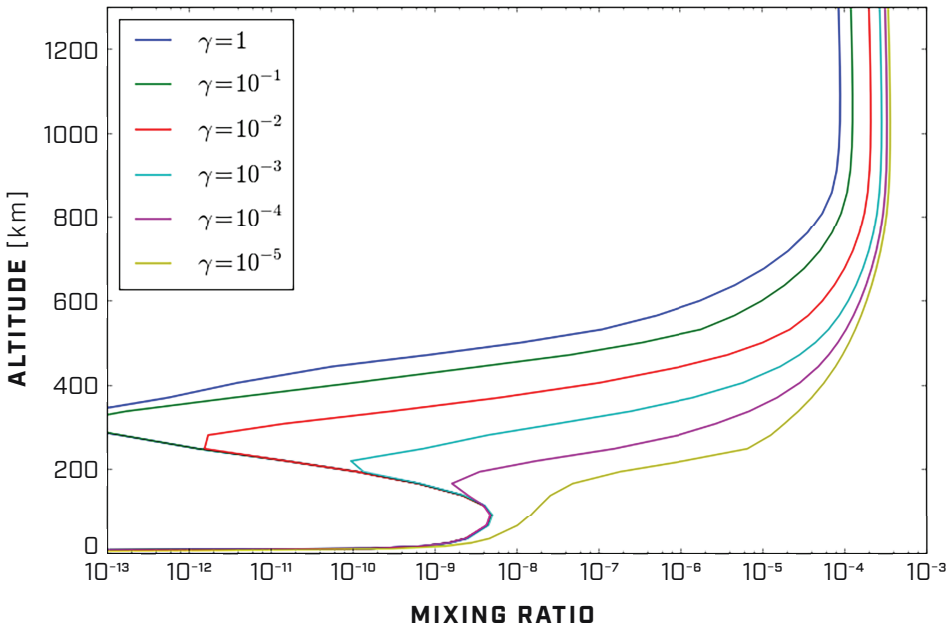

Figure 5. Various HCN profiles for a range of sticking coefficients γ_{HCN}. The greater the sticking coefficient, the more HCN condenses out of the atmosphere. The HCN column densities range from 1.2×10^{13} ($\gamma_{HCN} = 1$) to 1.2×10^{15} ($\gamma_{HCN} = 1 \times 10^{-5}$) molecules cm^{-2}. A sticking coefficient of $\gamma_{HCN} = 1 \times 10^{-2}$ gives an HCN column density of 4.8×10^{13} molecules cm^{-2}, which satisfies the value derived from ALMA observations (Lellouch et al. 2015).

3.4 PRECIPITATION RATES

Krasnopolsky and Cruikshank (1999) report perihelion precipitation rates for C_2H_2, C_4H_2, HC_3N, HCN, C_2H_6, and C_2H_4 of 195, 174, 69, 42, 27, and 18 g cm^{-1} Gyr^{-1}, respectively. For those same species, our photochemical model produces precipitation rates of 179, 26, 4, 35, 62, and 95 g cm^{-1} Gyr^{-1}. Our precipitation rates for the simpler C_2 hydrocarbons tend to be higher, and we attribute this to our more robust knowledge of their concentration profiles, which showed definite signs of condensation and informed our vapor pressure and sticking coefficient choices. As a consequence of removing the C_2 hydrocarbons faster, our model predicts a lower flux of higher-order hydrocarbons than Krasnopolsky and Cruikshank's (1999) model did. A list of the top 10 precipitating species in our model is presented in Table 1.

Species	Precipitation Rate [g cm^{-2} Gyr^{-1}]	Precipitation Rate K&C 1999 [g cm^{-2} Gyr^{-1}]
C_2H_2	179	195
C_2H_4	95	18
C_2H_6	62	27
CH_3C_2H	48	–
HCN	35	42
C_6H_6	34	–
C_4H_2	26	174
C_3H_6	8	–
CH_3C_2CN	6	–
HC_3N	4	69

Table 1. The top 10 precipitating species from this work with comparisons, where applicable, to Krasnopolsky and Cruikshank (1999).

3.4 OXYGEN CHEMISTRY

Despite there being very few observational constraints for oxygen-bearing species in Pluto's atmosphere, they must certainly be present, as carbon monoxide is the third most abundant gas. In our model, we set the surface mixing ratio of CO to 5×10^{-4} (Lellouch et al., 2011), and include an exogenous H_2O flux of $\sim 5 \times 10^5$ molecules cm^{-2} s^{-1} at the top of the atmosphere (Poppe, 2015). With these boundary conditions, our photochemical model predicts abundance profiles for oxygen-bearing molecules (Fig. 6) which may later be verified by future observations and data analysis.

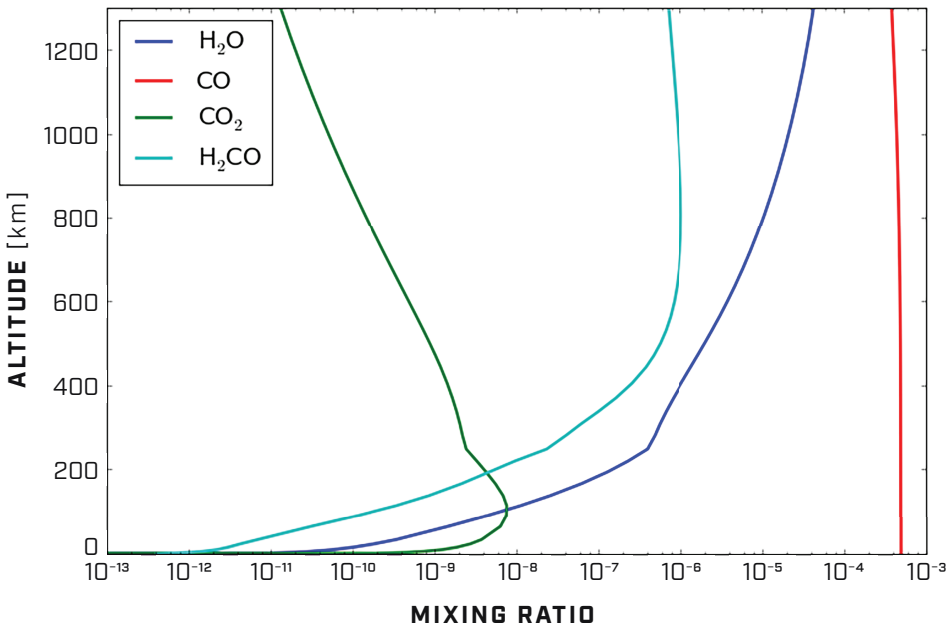

Figure 6. Model outputs for the major oxygen-bearing species in Pluto's atmosphere.

4. CONCLUSIONS

Although the atmospheres of Pluto and Titan share the same cast of characters—N_2, CH_4, CO, and their photochemical derivatives—the stories that they tell are different. Through linking specific unique outcomes with specific unique situational parameters, we can illuminate new knowledge about the physics and chemistry of planetary atmospheres. Each new planetary body that we visit is a brand new experiment that Nature has performed for our eyes to see and our minds to ponder. Pluto, the most distant object that humankind's mechanical proxies have encountered to date, represents Nature's laboratory for organic photochemistry at extremely low pressures and temperatures.

By fitting New Horizons' CH_4 profile, we gained knowledge about Pluto's eddy diffusion profile and surface CH_4 mixing ratio. By fitting New Horizons' C_2 hydrocarbon profiles, we learned about the saturation vapor pressures of C_2 hydrocarbons and their sticking coefficients at temperatures that have never been probed before. By fitting the HCN column density from ALMA observations, we have suggested a sticking coefficient for HCN as well. Finally, we make predictions for the abundances of oxygen-bearing species in Pluto's atmosphere. The proposed vapor pressure changes and the sticking coefficients could be tested by appropriate experiments in the laboratory, and future missions and observations can reveal Pluto's oxygen chemistry and validate or otherwise the results of this model.

ACKNOWLEDGEMENTS

This research was supported in part by a grant from the New Horizons mission. YLY and RLS were supported in part by the Cassini UVIS program via NASA Grant JPL.1459109, NASA NNX09AB72G grant to the California Institute of Technology. PG was supported in part by an RTD grant from JPL. MLW is grateful to Theater Arts at Caltech as a source of personal motivation by giving him the chance to portray Clyde Tombaugh in *Planet Between the Stars* during the course of this project.

Supersaturated water vapor as Pluto's mysterious atmospheric coolant

MICHAEL L. WONG[1], SITENG FAN[1],
KAREN WILLACY[2], PETER GAO[3], YUK L. YUNG[1,2]

[1]Division of Geological and Planetary Sciences, California Institute of Technology, Pasadena, CA 91125, USA
[2]Jet Propulsion Laboratory, California Institute of Technology, Pasadena, CA 91109, USA
[3]Department of Astronomy, University of California Berkeley, Berkeley, CA 94720, USA.

Unpublished manuscript

Among the avalanche of astonishing results from *New Horizons'* Pluto flyby in July 2015 was the discovery that Pluto's atmosphere was far colder and more compact than expected. Radio occultations performed by the REX instrument aboard *New Horizons* obtained the temperature structure of Pluto's atmosphere to unprecedented accuracy and resolution, revealing: a surface temperature buffered by the presence of N_2, CO, and CH_4 ices to ~37–45 K, a strong inversion that peaked at ~110 K around 50 km altitude, and an isothermal ~70 K upper atmosphere (Gladstone et al., 2016). This atmospheric structure is in stark contrast to atmospheres estimated from pre-*New Horizons* Earth-based observations, which were much more distended with a warm stratosphere of ~100 K that peaked in temperature at ~120 K near 450 km altitude (Krasnopolsky and Cruikshank, 1999). See Fig. 1 for a comparison of pre- and post-*New Horizons* temperature profiles.

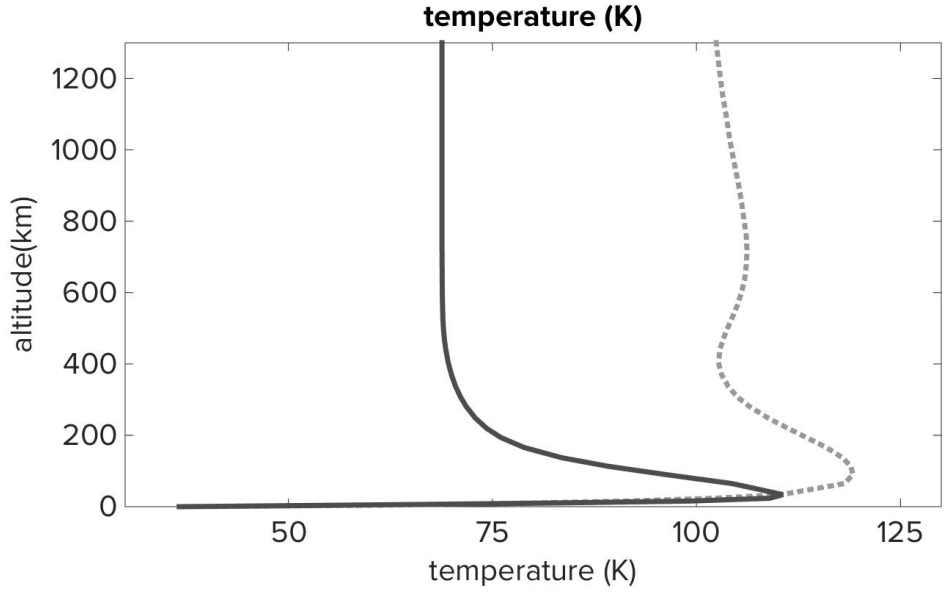

Fig. 1. Pluto's actual temperature profile (solid black) compared with its pre-New Horizons temperature profile (dashed gray).

The reality of a colder, more compact atmosphere has profound implications on the loss of N_2 from Pluto. Pre-*New Horizons* models forecasted N_2 hydrodynamically escaping Pluto's atmosphere at a rate of 2.8×10^{27} molecules s^{-1} (Zhu et al., 2014). However, the inferred N_2 escape rate based on *New Horizons* data is only 1×10^{23} molecules s^{-1}, which is satisfied by thermal Jeans escape (Gladstone, 2016), in contrast to nearly three decades of previous work on the possibility of hydrodynamic escape of N_2 from Pluto (Strobel and Zhu, 2017).

An unknown atmospheric coolant is responsible for the dramatic failure of all pre-*New Horizons* studies to predict the correct temperature of Pluto's upper atmosphere. This coolant radiates away in the thermal infrared the energy that might have been used to drive hydrodynamic escape. HCN has been proposed as the missing coolant in Pluto's atmosphere, but recent ground-based measurements limit the HCN in Pluto's atmosphere to insufficient abundance to serve as the main cooling agent (Strobel and Zhu, 2017). On the other hand, H_2O is a promising cooling candidate due to its rotational lines (Strobel and Zhu, 2017). Presently, there is no direct measurement of H_2O in Pluto's atmosphere, so H_2O as the missing coolant is a distinct possibility. Here, we quantitatively demonstrate that, if H_2O's sticking coefficient (defined as the fraction of collisions that result in sticking) is $\leq 1 \times 10^{-5}$, there can be enough H_2O vapor in Pluto's upper atmosphere to plausibly serve as the missing coolant.

Employing H_2O as the missing coolant requires supersaturated levels of H_2O, as illustrated in Fig. 2a. The required H_2O mixing ratio (orange) is ~10 orders of magnitude higher than the saturation vapor mixing ratio of H_2O (green) in the

upper atmosphere where cooling is most needed (see Figs. 6b and 7a of Strobel and Zhu, 2017, for details). H_2O supersaturation by 10 orders of magnitude may seem absurd, but there is observational evidence that HCN is similarly supersaturated in Pluto's atmosphere. Fig. 2b shows the mixing ratio of HCN (orange) that is compatible with recent microwave observations and the temperature profile observed by *New Horizons* (Lellouch et al., 2017); it is many orders of magnitude greater than the HCN saturation vapor mixing ratio (green). Lellouch et al. (2017) note that "the large abundance of HCN and the cold upper atmosphere imply supersaturation to a degree (7–8 orders of magnitude) hitherto unseen in planetary atmospheres." Furthermore, Rannou and West (2018) studied the microphysics of various types of nucleation and concluded that even in the case of heterogeneous nucleation onto aerosol particles with surface diffusion (the most effective removal mechanism considered), H_2O can exist at supersaturated levels in excess of 10^{10} at 200 km in Pluto's atmosphere.

In Fig. 2, we also show the expected chemical profiles (blue) from Wong et al.'s (2016) photochemical model, which took into account HCN condensation, but not H_2O condensation. The source of H_2O in the Wong et al. (2017) model was ablation from Kuiper Belt dust grains falling into Pluto's atmosphere, engendering an H_2O flux of 5×10^5 molecules cm^{-2} s^{-1}, as implied by the *New Horizons* Student Dust Counter (SDC) experiment (Poppe, 2015). As the Wong et al. (2017) model did not consider any condensation processes for H_2O, any apparent agreement between this model and the abundance of H_2O necessary to

cool Pluto's atmosphere is purely accidental. In order to validate or refute the possibility of H_2O as the missing coolant, we must consider H_2O condensation.

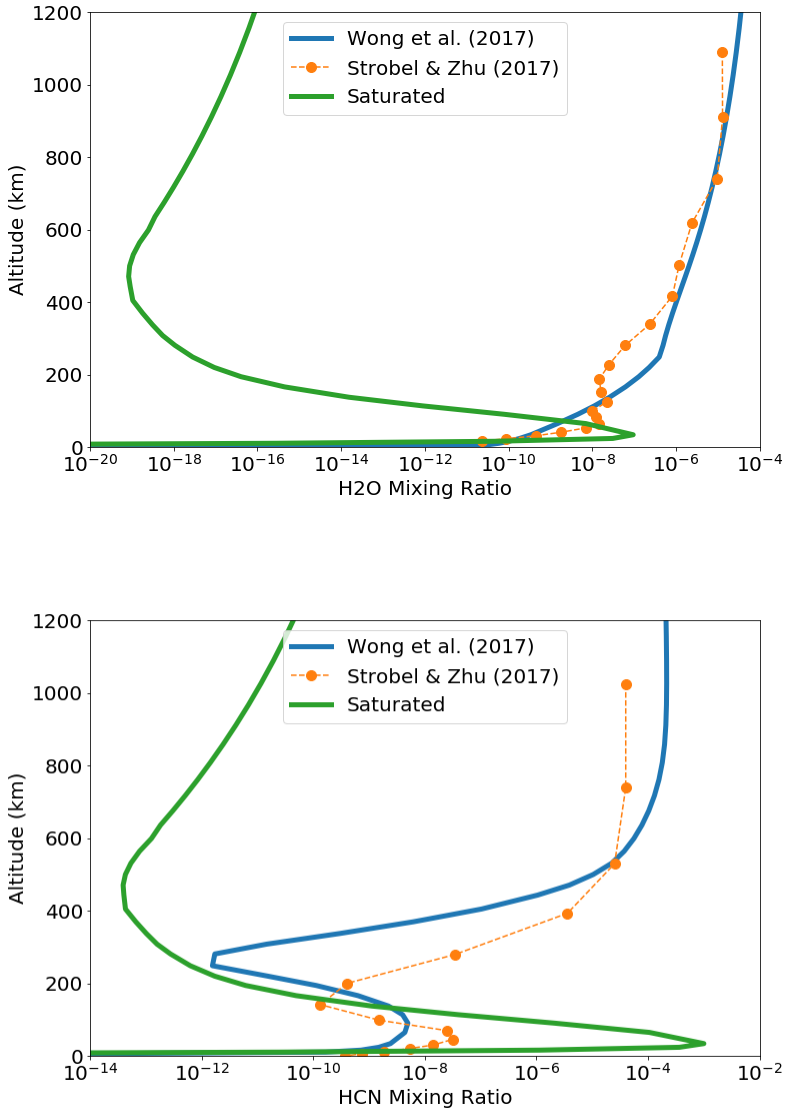

Fig. 2 Mixing ratio profiles for **(a)** H_2O and **(b)** HCN. **Blue** lines represent the mixing ratio from Wong et al.'s (2017) photochemical model. For H_2O, no condensation is assumed. For HCN, a sticking coefficient of 1 × 10^{-2} is used. **Green** lines represent the saturation vapor pressure of the respective species. **Orange** dots represent **(a)** the profile of H_2O that Strobel & Zhu (2017) derived to cool Pluto's atmosphere and **(b)** the observed HCN profile via ALMA observations reported in Lellouch (2017) and plotted in Strobel & Zhu (2017).

This work presents an updated Pluto photochemical model that takes into account removal of H_2O from Pluto's atmosphere via heterogeneous condensation. As discussed in Wong et al. (2017), heterogeneous condensation onto fractal

aggregate haze particles determines the concentration profiles of gaseous hydrocarbon and nitrile species and their overall abundances in Pluto's atmosphere.

Consider a parcel of plutonian air containing various gaseous species x with number densities n_x. Each gas molecule has a characteristic gas phase velocity v_x. The air parcel also contains aerosol particles at a number density of n_a. Each aerosol particle presents a cross-sectional area σ_a. Collisions between molecules of x with aerosol particles happens at a rate of $\sigma_a n_a n_x v_x$ molecules cm^{-3} s^{-1}, but not all collisions result in condensation. For sticking to occur, a requisite number of gas molecules must accumulate on the surface of the grain to form a critical cluster. This microphysical process is parameterized by a sticking coefficient $S_x \leq 1$. Thus, the heterogeneous condensation rate of a given gaseous species x onto an aerosol is described by

$$R_c = S_x \sigma_a n_a n_x v_x \text{ molecules cm}^{-3} \text{ s}^{-1}. \quad (1)$$

The sublimation rate of volatiles from the aerosol particles in our parcel of air depends on the number density of aerosol particles n_a, the 3-D surface area of each aerosol $4\sigma_a$ particle, and the sublimation rate coefficient k_s (molecules cm^{-2} s^{-1}):

$$R_s = k_s 4\sigma_a n_a \text{ molecules cm}^{-3} \text{ s}^{-1}. \quad (2)$$

Gao et al. (2016) calculated the quantity $\sigma_a n_a$ for Pluto's atmosphere for conditions contemporaneous with *New Horizons*' flyby. n_x is calculated at each time step of our photochemical model. v_x is given by the thermal velocity $v_{th} \sim \sqrt{k_b T/m}$, where k_b is Boltzmann's constant, T is the measured temperature of the atmosphere, and m is the mass of the gas particle in question. S_x is our free parameter.

The only unknown is the sublimation rate coefficient k_s, but that can be solved for by knowing that at equilibrium, by definition, $R_c = R_s$, and n_x is at its saturation vapor density, n_x^{sat}, as determined by laboratory studies. Thus, at equilibrium,

$$S_x \sigma_a n_a n_x^{sat} v_x = k_s 4 \sigma_a n_a. \quad (3)$$

Rearranging,

$$k_s = \frac{1}{4} S_x n_x^{sat} v_x \text{ molecules cm}^{-2} \text{ s}^{-1}. \quad (4)$$

Substituting Equation 4 into Equation 2 results in

$$R_s = S_x \sigma_a n_a n_x^{sat} v_x \text{ molecules cm}^{-3} \text{ s}^{-1}. \quad (5)$$

The net condensation rate is

$$R_{net} = R_c - R_s = S_x \sigma_a n_a v_x (n_x - n_x^{sat} \Theta_x) \text{ molecules cm}^{-3} \text{ s}^{-1}, \quad (6)$$

where Θ_x is the fraction of binding sites on the aerosol particle that is occupied by volatile species x. Θ_x can be calculated by

$$\Theta_x = {n_x^{cond}}\Big/{\sum_y n_y^{cond}}, \quad (7)$$

where n_x^{cond} is the number density of species x in the condensed phase and $\sum_y n_y^{cond}$ represents the total number density of all molecules condensed on the grain surface.

Equations 6 and 7 can also be found as Equations 9 and 10 in Willacy et al. (2016).

Using this formalism, we are able to compute the removal of gaseous species in Pluto's atmosphere due to heterogeneous condensation onto aerosols. We vary our one free parameter, the sticking coefficient S_x, and solve for the vertical profiles and column abundances of relevant species. For example, Wong et al. (2017) determined that the HCN profile that best matched the AMLA observations required $S_{HCN} = 1 \times 10^{-2}$.

The reason behind HCN's extreme supersaturation is that the timescale for removal by heterogeneous condensation is much longer than the timescale for vertical transport. Here we define the removal time $\tau_{removal} \sim J^{-1}$ as the inverse of the sticking rate coefficient *J*, defined by

$$J = S_x v_x \sigma_a n_a \,, \tag{8}$$

as in Equation 3 of Wong et al. (2017). The characteristic timescale for vertical transport is defined by

$$\tau_{transport} \sim \frac{H^2}{K_{zz}+D}, \tag{9}$$

where H is the atmospheric scale height, K_{zz} is the eddy diffusion coefficient, and D is the molecular diffusion coefficient.

Fig. 3 shows that for HCN and a sticking coefficient of 1×10^{-2}, the characteristic time for transport by molecular and eddy diffusion above 400 km is significantly shorter than that for removal by sticking to an aerosol. Indeed, in the limit of a very low sticking coefficient, transport dominates over removal by sticking, thus creating extremely large supersaturation.

In this study, we extend the work of Wong et al. (2017) and model the condensation of H_2O vapor in Pluto's atmosphere. Fig. 3 also compares the timescale for condensation and the timescale for vertical transport for H_2O. Fig. 4 shows various H_2O profiles for a range of S_{H_2O}. Like HCN, H_2O can also be elevated to high levels of supersaturation given low enough sticking coefficients. As can be seen in Fig. 4, to reach the level of supersaturation required to explain Pluto's cooling via H_2O rotational line emission (the black dots in Fig. 4), $S_{H_2O} \leq 1 \times 10^{-5}$.

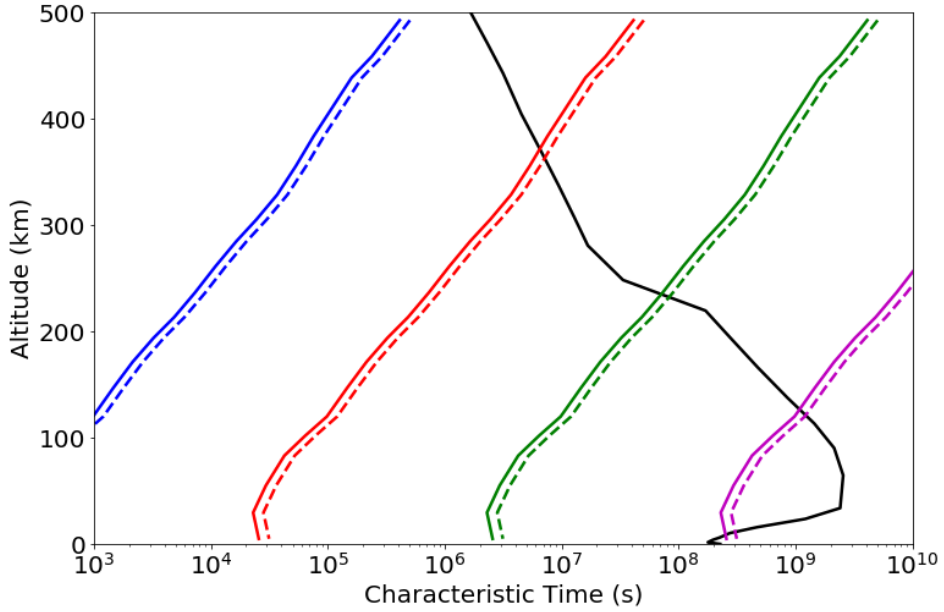

Fig. 3. The characteristic timescale for vertical transport via molecular and eddy diffusion (black) vs. the characteristic timescale for heterogeneous condensation of H_2O (solid) and HCN (dashed) given various sticking coefficients (blue: $S_x = 1$; red: $S_x = 10^{-2}$; green: $S_x = 10^{-4}$; purple: $S_x = 10^{-6}$).

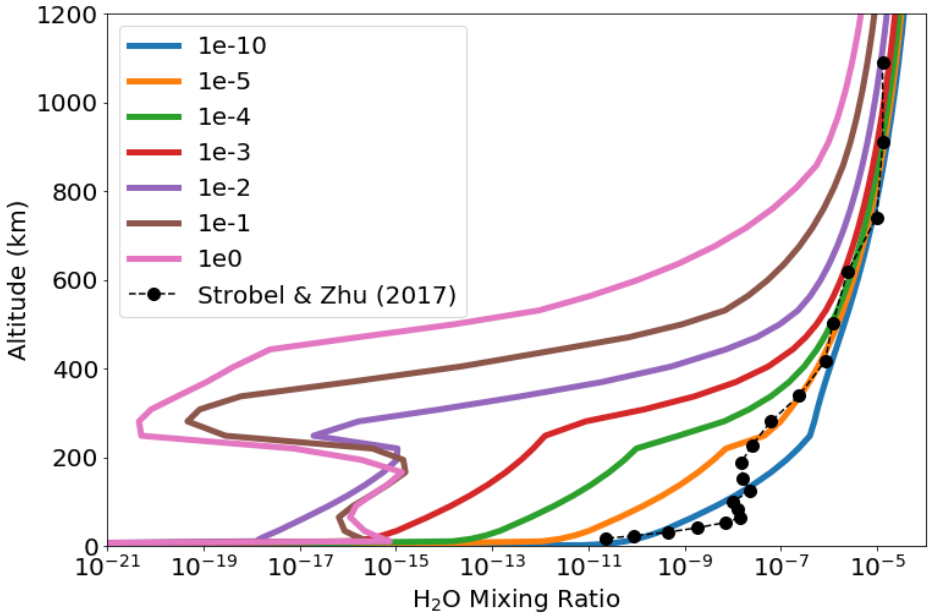

Fig. 4. Various H2O mixing ratio profiles for different sticking coefficients compared with the required H2O profile to cool Pluto's atmosphere from Strobel & Zhu (2017).

Zhang et al. (2017) present an alternate explanation where haze particles provide the majority of the thermal cooling in Pluto's atmosphere. If this is true, then it sets Pluto apart as the only Solar System body whose radiative energy equilibrium is controlled primarily by haze particles rather than by gas molecules. There is still a wide uncertainty in the radiative properties of Pluto's haze, however, as haze optical constants are influenced by the specifics of formation chemistry and their ultimate chemical structures. It could be that Pluto's haze material differs from that of Titan in ways that make Titan tholin experiments poor analogs for Pluto. Furthermore, as Wong et al. (2017) and Gao et al. (2017) suggest, Pluto haze particles play an important role in seeding the condensation of hydrocarbons and HCN. As these haze particles descend and become coated with gas molecules that adsorb onto their surfaces, their optical properties are likely to change. Thus, we consider the work of Zhang et al. (2017) to be a possible but not definitive solution to the cooling of Pluto's atmosphere. It could be that hazes and H_2O may both play a substantial role in cooling Pluto's atmosphere. Future observations (such as by the forthcoming James Webb Space Telescope) may verify Zhang et al.'s (2017) hypothesis by detecting the radiation flux to space from hazes or detect H_2O molecules in supersaturated abundance in line with this work.

In conclusion, we have shown that H_2O, ablated from an influx of Kuiper Belt dust, could exist at high enough abundances to explain the unexpectedly cold

temperatures of Pluto's atmosphere. If the H_2O sticking coefficient S_{H_2O} is as low as 1×10^{-5}, the timescale for heterogeneous condensation of gaseous H_2O molecules onto fractal aggregate haze particles is much lower than the vertical transport timescale, allowing for enough H_2O vapor to exist in Pluto's atmosphere to cool it to observed temperatures via rotational line emission. H_2O molecules that do condense onto haze particles should be released when the haze particles encounter Pluto's warm lower atmosphere, rejuvenating the reservoir of H_2O vapor. If H_2O is indeed the missing coolant, then it would explain the failure of all pre-*New Horizons* models to predict the atmospheric structure, chemistry, and escape rates that were observed during *New Horizons'* extraordinary encounter with Pluto.

CHAPTER III

LOOKING FOR A PLACE TO REST

Nitrogen Oxides in Earth's Early Atmosphere as Electron Acceptors for Life

MICHAEL L. WONG[1], BENJAMIN D. CHARNAY[2,3], PETER GAO[4], YUK L. YUNG[1,5], AND MICHAEL J. RUSSELL[5]

[1]*Division of Geological and Planetary Sciences, California Institute of Technology, Pasadena, CA 91125, USA*
[2]*LESIA, Observatoire de Paris, PSL Research University, CNRS, Sorbonne Universités, UPMC Univ. Paris 06, Univ. Paris Diderot, Sorbonne Paris Cité, Meudon, France*
[3]*Virtual Planetary Laboratory, University of Washington, Seattle, WA 98195, USA*
[4]*Department of Astronomy, University of California Berkeley, Berkeley, CA 94720, USA.*
[5]*Jet Propulsion Laboratory, California Institute of Technology, Pasadena, CA 91109, USA*

Published in *Astrobiology*
Vol. 17, No. 10, pp. 975–983
October 1, 2017

ABSTRACT

We quantify the amount of nitrogen oxides (NOx) produced through lightning and photochemical processes in the Hadean atmosphere to be available in the Hadean ocean for the emergence of life. Atmospherically generated nitrate (NO_3^-) and nitrite (NO_2^-) are the most attractive high-potential electron acceptors for pulling and enabling crucial redox reactions of autotrophic metabolic pathways at submarine alkaline hydrothermal vents. The Hadean atmosphere, dominated by CO_2 and N_2, will produce nitric oxide (NO) when shocked by lightning. Photochemical reactions involving NO and H_2O vapor will then produce acids such as HNO, HNO_2, HNO_3, and HO_2NO_2 that rain into the ocean. There, they dissociate into or react to form nitrate and nitrite. We present new calculations based on a novel combination of early-Earth GCM and photochemical modeling, and predict the flux of NOx to the Hadean ocean. In our 0.1-, 1-, and 10-bar pCO_2 models, we calculate the NOx delivery to be 2.4×10^5, 6.5×10^8, and 1.9×10^8 molecules cm^{-2} s^{-1}. After only tens of thousands to tens of millions of years, these NOx fluxes are expected to produce sufficient (micromolar) ocean concentrations of high-potential electron acceptors for the emergence of life.

1. INTRODUCTION

Nitrogen oxides (NOx)—formed by lightning discharges and photochemistry in the Hadean atmosphere and rained out into the all-enveloping Hadean ocean—may have played a vital role in the emergence and early evolution of life on Earth (Mancinelli and McKay, 1988). In particular, the high-potential electron acceptors nitrate (NO_3^-) and nitrite (NO_2^-) could conceivably have initiated the first metabolic pathway through the oxidation of hydrothermal CH_4 and the concomitant hydrogenation of CO_2 at ancient submarine alkaline hydrothermal vents (Ducluzeau et al., 2009; Nitschke and Russell, 2013; Shibuya et al., 2016).

In contrast to the renowned magma-driven "black smoker" (350–400 °C, pH ~3) springs, Hadean alkaline hydrothermal systems would have been powered by the geothermal gradient, augmented by exothermic serpentinization of the mainly peridotitic crust (Table 1). Their effluents would have been only moderately hot (≤92 °C), but also alkaline (pH ~11). These fluids would have reacted with the then acidic ocean to produce porous submarine hydrothermal mounds (Russell, Hall, & Martin, 2010).

The present-day hydrothermal vents at Lost City, where fluid exhalation temperatures reach 92 °C at a pH of ~11, provide a modern analog (Kelley et al., 2001; Martin et al., 2008; Seyfried et al., 2015). While brucite ($Mg[OH]_2$) is a major initial component of Lost City mounds, owing to the high concentration of Mg in the present-day ocean, Hadean mounds would have had an iron-dominated mineralogical composition. The Hadean ocean was carbonic and rich in iron and

other transition metals, so the porous precipitate mounds would have comprised amorphous to microcrystalline brucite-structured iron oxyhydroxides or green rusts (e.g., ~ $Fe^{II}_4Fe^{III}_2(OH)_{12}][CO_3]\cdot 3H_2O$) along with the iron sulfides mackinawite and greigite, dosed with nickel, cobalt, and molybdenum (Génin et al., 2005; Génin et al., 2006; Mloszewska et al., 2012; Nitschke & Russell, 2013; Russell & Hall, 1997; Russell et al., 2014; White et al., 2015).

Acidic vents	**Alkaline vents**
Ocean Ridge	Off-ridge, Peridotite-hosted
Driven by magmatic intrusion	Driven by exothermic serpentinization
T ~ 400 ºC	T ~ 130 ºC
pH ~3	pH ~ 11

Table 1. Alkaline (e.g. Lost City) versus acidic ("black smoker") hydrothermal vents. Acidic vents are thought to be too hot and acidic for the emergence of life, but alkaline mounds offer a promising milieu for the first metabolic pathways. In addition to their innate electro-geochemical gradients imposed across their margins, submarine alkaline hydrothermal vents provide the fuels H_2 and CH_4, ambient electron acceptors in the form of nitrate, nitrite and ferric iron, and a powerful suite of mineral catalysts that resemble the Fe/Ni clusters in enzymes that promote metabolism in life today (Martin et al., 2008; Proskurowski et al., 2006; Seyfried et al., 2015).

Electro-geochemical gradients would have been imposed across inorganic precipitates between the mildly acidic, CO_2-rich Hadean seawater and the alkaline hydrothermal fluid laden with H_2 and CH_4, products of serpentinization and hydrothermal leaching, respectively (Russell et al., 1989; Barge et al., 2015). Nitschke and Russell (2013) suggested that the first carbon fixation pathway operated through the process of denitrifying methanotrophic acetogenesis—a

putative variant of the ancient acetyl-coenzyme A pathway still used by anaerobic microbes—in which H_2 reduces CO_2 to CO, and CH_4 is oxidized through methanol to a methylene entity before being reduced and thiolated to give CH_3SH. The CO and CH_3SH react on an iron-nickel sulfide to produce activated acetate (Huber and Wächtershäuser, 1997). Thereafter, more complex biomolecules are formed through a series of hydrogenations, carboxylations, aminations, and condensations (Huber and Wächtershäuser, 2003; Kawamura et al., 2011). The eventual waste product is acetate (CH_3COO^-) (Russell & Martin, 2004).

However, this scheme cannot proceed unassisted; CH_4 and CO_2 are each notoriously unreactive molecules. The high-potential electron acceptors nitrate and/or nitrite perform two crucial roles in the earliest carbon fixation engines of life by providing the following: 1) the required extra disequilibrium to activate CH_4, which is converted into methanol as nitrate/nitrite is re-reduced to NO (Nitschke and Russell, 2013) and 2) redox bifurcate electrons by coupling the acceptance of one of two outer shell molybdenum electrons, as the other reduces the low-potential electron acceptor CO_2 to CO (Helz et al., 2014; Nitschke and Russell, 2013; Schoepp-Cothenet et al., 2012) (Fig. 1).

Additionally, nitrate and/or nitrite represents a form of fixed nitrogen that could have been reduced to ammonium for proto-biosynthesis in the otherwise inorganic membranes surrounding compartments in the Hadean hydrothermal mound. In the interlayers of green rust, carbonate, sulfide, and chloride are stable as intercalates, but nitrate and nitrite are reduced to ammonium (NH_4^+) in a matter of hours (Hansen et al., 2001; Trolard & Bourrié, 2012). Ammonium is a key

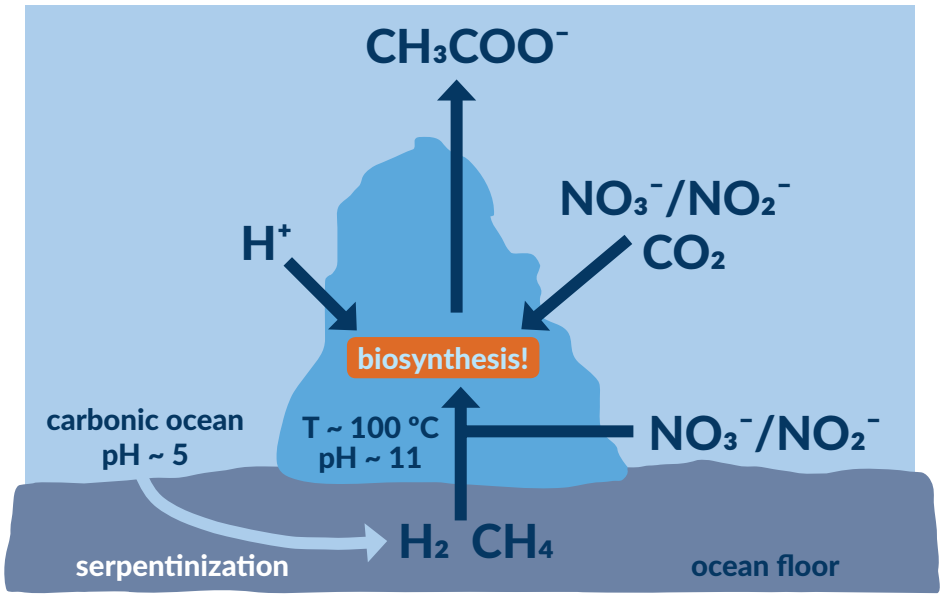

Fig. 1. The first metabolic engines would have "burned" hydrothermal fuels H_2 and CH_4 with the NO_3^-, NO_2^-, and CO_2 found in early Earth's carbonic ocean (Branscomb and Russell, 2013; Nitschke and Russell, 2013). Nitrate and/or nitrite would be necessary to reduce CO_2 to CO and oxidize CH_4 to a methyl group. An excess of H^+ outside of the chimney produces a steep pH gradient—a natural proton motive force with the same directionality as the proton motive force driving metabolic pathways and cycles operating universally across biology to this day.

ingredient for building amino acids from α-carboxylic acids in the presence of mixed ferrous–ferric hydroxides—critical for turning a primitive metabolic pathway into a ligand-accelerated autocatalytic system (Huber and Wächtershäuser, 2003; Milner-White and Russell, 2008; Russell et al., 2014; White et al., 2015). For example, pyruvate, in the presence of NH_4^+, can be aminated to alanine (Huber & Wächtershäuser, 2003). Alanine could then have condensed to a 5-mer peptide on carbonate surfaces in the mound (Kawamura et al., 2011). Such peptides have the potential to render iron-nickel sulfides and pyrophosphate clusters more stable and catalytically active, thus quickening the reactions along the pathway that had

previously relied on the unadorned inorganic clusters themselves (Milner-White and Russell, 2011; Bianchi et al., 2011). Such a positive feedback would lock this cycle in as the foundation for an autocatalytic pathway at the emergence of life (e.g., Mielke et al., 2011).

Given the important role nitrogen oxides might have played at life's emergence—both as vital high potential electron acceptors and as the main source of fixed nitrogen to emerging biosynthesis—it behooves us to ascertain whether the production of NOx in the Hadean atmosphere would produce sufficient concentrations of nitrate and nitrite in the Hadean ocean to meet model requirements.

The Hadean, which spans the first half billion years of Earth's history, was a tumultuous time. The planet was bombarded by bolides and singed by the young Sun's intense ultraviolet radiation. Days were only ~14 hours long, massive tides were induced by a closer Moon, and continents did not exist. The ocean was twice its present volume, and the atmosphere was suffused with the products of ubiquitous volcanism (Russell et al., 2014, and references therein).

Although geochemical evidence points to an atmosphere dominated by CO_2 and N_2, it is still uncertain how massive the atmosphere was. Indeed, it is likely to have varied greatly during the Hadean eon under the vagaries of bolide collisions, mantle convective overturn, and accompanying tectonics. After the magma ocean phase and the condensation of ocean, Earth's atmosphere was likely composed of around 50 bars of CO_2. This pressure decreased quickly with the formation of carbonates at the seafloor. Sleep et al. (2001) estimated that the partial pressure of

CO_2 (pCO_2) was 5–20 bars during the first 1–20 Myr. Afterwards, pCO_2 decreased to an equilibrium value that is still unknown. Ongoing work coupling GCMs to carbon cycling models result in a Hadean pCO_2 between 0.1 and 0.5 bar, depending on the continental cover and the recycling in the subduction (Charnay, 2016, private communication).

To determine the abundance of NOx on the early Earth, we must address a wide range of atmospheric pressures. In this study, we test CO_2 partial pressures of 0.1, 1, and 10 bars, complemented by 1 to 2 bars of N_2.

2. ESTIMATES OF LIGHTNING & LIGHTNING-INDUCED NO

Along with the contribution from volcanic activity (Martin, Mather, & Pyle, 2007), lightning is the main source of nitrogen oxides (Schumann and Huntrieser, 2007) generated in the lower atmosphere. For simplicity, we ignore nitrogen fixation caused by coronal mass ejection events from the Sun (Airapetian et al., 2016). On the oxygen-rich present-day Earth, ~300 moles of NO are generated per lightning flash (Choi et al., 2009), corresponding to a lightning-induced NO flux of ~6×10^8 molecules cm^{-2} s^{-1}. In the anoxic early atmosphere, electrical discharges would have heated air temperatures to tens of thousands of kelvin and incited the normally unsociable molecules CO_2 and N_2 to react. Electrical-discharge events shatter the robust covalent double bonds of CO_2, splitting CO_2 into CO and O. The highly reactive O radical breaks N_2's triple bond, producing NO (nitric oxide) and N. The

N radical then goes on to react with another CO_2 molecule, creating CO and even more NO (Ducluzeau et al., 2009; Nna Mvondo et al., 2001). The process can be summarized as:

$$CO_2 \longrightarrow CO + O,$$

$$O + N_2 \longrightarrow NO + N,$$

$$N + CO_2 \longrightarrow NO + CO.$$

This lightning-induced NO is the fundamental source of all higher-order NOx generated by photochemistry.

To estimate the amount of lightning-induced NO in the Hadean, we must first estimate the amount of lightning in the Hadean. Romps et al. (2014) derived the most accurate predictor of lightning flash rate to date:

$$F = \frac{\eta}{E} \times P \times \mathrm{CAPE}\,,$$

where F is the lightning flash rate per area (flashes m^{-2} s^{-1}), P is the precipitation rate (kg m^{-2} s^{-1}), and CAPE is the convective available potential energy. This formula is valid in GCMs where P and CAPE are derived in a cell where there is a convective cloud. We assume that the constant of proportionality, η/E, which contains the efficiency η (the ratio of power per area dissipated by lightning to the CAPE per area per time available to condensates) and the energy discharge per

flash E (joules), to be the same as today. We assume the present-day average lightning discharge energy $E \sim 5 \times 10^9$ J flash^{-1}. Thus,

$$F \propto P \times \mathrm{CAPE} .$$

We run the Generic LMDZ 3-D global climate model (GCM) to compute P and CAPE for early Earth, which allows us to scale the present-day average lightning flash rate (1.1 flashes km^{-2} yr^{-1}) to that of an early-Earth atmosphere. The Generic LMDZ 3-D GCM has a universal dynamic core, a correlated-k radiative transfer code, universal turbulence and robust convection schemes in the lower atmosphere, volatile condensation in the atmosphere and surface, a 2-layer dynamic ocean, and surface and subsurface thermal balance. It has been used to great effect in studies of other planetary scenarios, including Archean Earth (Charnay et al., 2013), early Mars (Forget et al., 2013), and even terrestrial-mass exoplanets (Wordsworth et al., 2011).

The computed lightning flash rates are 0.41, 9.3, and 3.1 flashes km^{-2} yr^{-1} for the 0.1-, 1-, and 10-bar pCO_2 cases, respectively. An increase in the global mean surface temperature should enhance the frequency and power of convective storms and thus enhance the lightning flash rate (Romps et al., 2014). As expected, our model produces a higher lightning flash rate for the 1-bar pCO_2 case (mean surface temperature of 332.8 K) than for the 0.1-bar pCO_2 case (280.4 K). Surprisingly, the 10-bar pCO_2 (388.1 K) case has a lower flash rate than the 1-bar pCO_2 case.

The 10-bar pCO_2 case features the warmest troposphere. Hence, the lower atmosphere is rich in water vapor, making it extremely opaque (only 7 W/m^2 of sunlight reaches the surface). The absorption of solar radiation in the atmosphere and a strong thermal inversion above the surface, as expected for very warm and moist climates (Pierrehumbert, 2010, p. 418), stabilizes the atmosphere against moist convection. Though the precipitation rate in the 10-bar case (5.1 mm/day) is comparable to that of the 1-bar case (5.8 mm/day), there are few convective clouds and the CAPE is low, effectively suppressing the lightning flash rate by a factor of 3.

Using empirical data for NO yield with respect to different CO_2–N_2 mixtures (Nna Mvondo et al., 2001) (reproduced here in Fig. 2), and $E \sim 5 \times 10^9$ J flash^{-1}, we are able to calculate a lightning-induced NO flux for each pCO_2 (see Table 4).

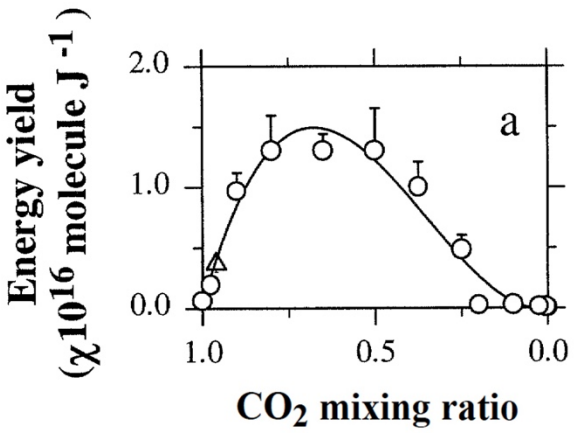

Fig. 2. A reproduction of Fig. 1a from Nna Mvondo et al. (2001) showing the NO yield per J of lightning for various mixtures of CO_2 and N_2. The circles are Nna Mvondo's data points; the triangle is an experimental result from Venusian lightning (Levine et al., 1982) for comparison. After calculating lightning flash rates for our 0.1-, 1-, and 10-bar pCO_2 cases, we use this plot to evaluate the lightning-generated NO flux in the troposphere for each case. Although we take this data as ground truth for our study, we hope that future work (either experimental or theoretical) will confirm, or otherwise, the results in this plot.

3. PHOTOCHEMICAL PRODUCTION OF NOx

To evaluate the production of NOx species in the Hadean atmosphere, we adapt the 1-D Caltech/JPL chemical transport model (Allen et al., 1981) to simulate the Hadean Earth. Other versions of this model have been well tested on numerous planetary bodies, including Jupiter, Titan, and Pluto (see, e.g., Wong, Yung, & Gladstone, 2015). In our early-Earth model, we simulate 28 chemical species and 156 chemical reactions. The model calculates the chemical production and loss rates at each altitude as well as the diffusive flux between each altitude grid by solving the 1-D continuity equation:

$$\frac{dn_i}{dt} = P_i - L_i - \frac{\partial \varphi_i}{dz},$$

where n_i is the number density of species i, φ_i the vertical flux, P_i the chemical production rate, and L_i the chemical loss rate, all evaluated at time t and altitude z. The vertical flux is given by

$$\varphi_i = -\frac{\partial n_i}{dz}(D_i + K_{zz}) - n_i\left(\frac{D_i}{H_i} + \frac{K_{zz}}{H_{atm}}\right) - n_i \frac{\partial T}{\partial z}\left[\frac{(1+\alpha_i)D_i + K_{zz}}{T}\right],$$

where D_i is the species' molecular diffusion coefficient, H_i the species' scale height, H_{atm} the atmospheric scale height, α_i the thermal diffusion coefficient, K_{zz} the vertical eddy diffusion coefficient, and T the temperature (Yung and DeMore, 1999).

The atmospheric temperature profiles for our photochemical runs are based on those obtained from the GCM's output. The temperature decreases with altitude, following a wet adiabat from the surface to mesosphere, where it becomes isothermal. We calculate the eddy diffusion coefficient profile using the formulation in the work of Ackerman & Marley (2001). Fig. 3 shows the temperature and eddy diffusion coefficient profiles of all three cases.

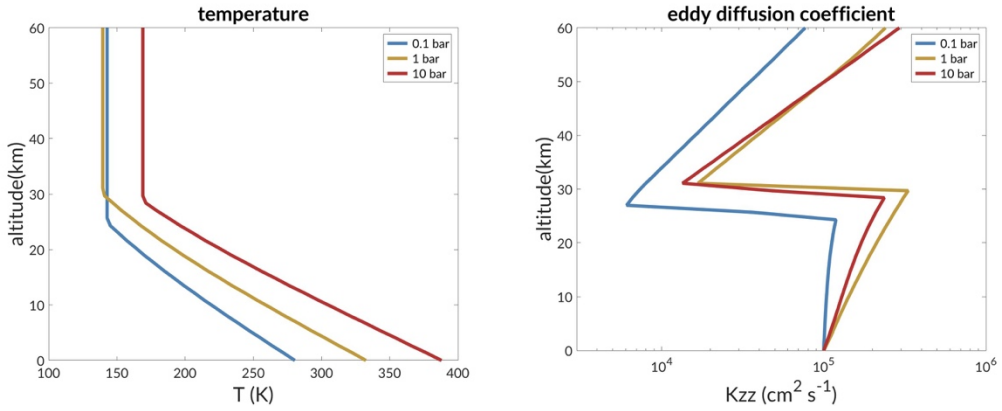

FIG. 3. (a) The atmospheric temperature profiles of the 0.1-, 1-, and 10-bar pCO_2 cases. **(b)** The eddy diffusion coefficient profiles of the 0.1-, 1-, and 10-bar pCO_2 cases, calculated using Equation 5 of Ackerman and Marley (2001), starting from an assumed surface value of 1×10^5 cm^2 s^{-1}. The inversion feature exhibited by all three cases corresponds to the location of the tropopause, as defined by the temperature profile.

In the lowest atmospheric level, which extends from 0 to 1.4 km, we inject an NO flux corresponding to our calculations for lightning-induced NO production. We assume a surface H_2 mixing ratio of 1×10^{-3}, corresponding to a volcanically active, weakly reduced early Earth (Kasting, 1993).

The bulk of our photochemical scheme is based upon the Nair et al. (1994) model for Mars's CO_2–N_2 atmosphere, updated to include HNO and a new

formation pathway for HNO_3 (discussed later in this section). The additional reactions are listed in Table 2. Unlike the Nair et al. (1994) model, our model atmospheres are irradiated by the faint young Sun (Claire et al., 2012), and the updated photolysis rates at the top of the atmosphere (100 km) are calculated and catalogued in Table 3.

Reaction	Rate constant *k*	Reference
$H + NO + M \longrightarrow HNO + M$	$2.1 \times 10^{-32}\ e^{300/T}$	Hampson and Garvin (1977)
$H + HNO \longrightarrow H_2 + NO$	7×10^{-12}	Hampson and Garvin (1977)
$OH + HNO \longrightarrow H_2O + NO$	$8 \times 10^{-11}\ e^{-500/T}$	Tsang and Herron (1991)
$HO_2 + NO + M \longrightarrow HNO_3 + M$	$3.5 \times 10^{-14}\ e^{250/T}$	Butkovskaya et al. (2007)

Table 2. Additional reactions involving HNO and HNO_3, and their corresponding rate coefficients, to the Nair et al. (1994) model. The units for two-body and three-body reactions are $cm^3\ s^{-1}$ and $cm^6\ s^{-1}$, respectively.

Reaction	Photolysis rate coefficient at 100 km (s^{-1})
$O_2 + h\nu \longrightarrow O + O$	2.71×10^{-6}
$O_2 + h\nu \longrightarrow O + O(^1D)$	1.10×10^{-5}
$O_3 + h\nu \longrightarrow O_2 + O$	3.68×10^{-4}
$O_3 + h\nu \longrightarrow O_2 + O(^1D)$	9.16×10^{-7}
$H_2O + h\nu \longrightarrow H + OH$	3.03×10^{-5}
$NO + h\nu \longrightarrow N + O$	3.50×10^{-6}
$NO_2 + h\nu \longrightarrow NO + O$	2.74×10^{-3}
$NO_3 + h\nu \longrightarrow NO_2 + O$	5.26×10^{-2}
$NO_3 + h\nu \longrightarrow NO + O_2$	7.63×10^{-3}
$N_2O + h\nu \longrightarrow N_2 + O(^1D)$	1.33×10^{-5}
$HNO + h\nu \longrightarrow H + NO$	1.70×10^{-3}
$HNO_2 + h\nu \longrightarrow OH + NO$	6.04×10^{-4}
$HNO_3 + h\nu \longrightarrow OH + NO_2$	5.72×10^{-5}
$HO_2NO_2 + h\nu \longrightarrow HO_2 + NO_2$	9.59×10^{-5}
$CO_2 + h\nu \longrightarrow CO + O$	3.31×10^{-7}
$CO_2 + h\nu \longrightarrow CO + O(^1D)$	5.68×10^{-7}

Table 3. Updated Nair et al. (1994) photolysis rate coefficients at the top of the atmosphere. Other than the rate coefficient for $HNO + h\nu \longrightarrow H + NO$, which was taken from Kasting and Walker (1981), these rate coefficients

were computed by our model from the known photochemical cross sections and the solar flux of the faint young sun.

Our model calculates and outputs chemical abudances for each species at every level. The vertical profiles of photochemically derived O_2, NOx, and N_2O in the 1-bar pCO_2 case are presented in Fig. 4.

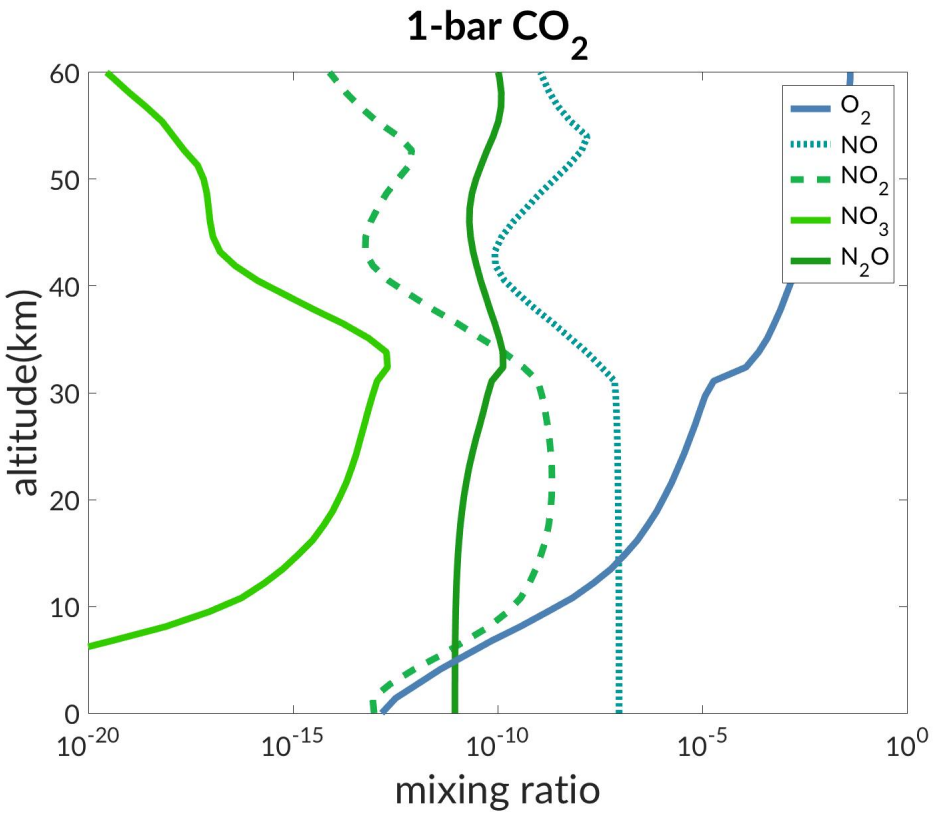

Fig. 4. The mixing ratio profiles of O_2, NOx, and N_2O for the 1-bar pCO_2 case.

The rainout rates for various electron acceptors are summarized in Fig. 5 and Table 4. Among the NOx species, in all three cases, the flux of HNO rain is the highest, followed by HNO_3, HO_2NO_2, and HNO_2. Across all species, the

highest rainout rate is produced in the 1-bar pCO_2 case. The total amount of NOx rained out into the Hadean ocean is 2.4×10^5, 6.5×10^8, and 1.9×10^8 molecules cm^{-2} s^{-1} for the 0.1-, 1-, and 10-bar pCO_2 cases, respectively.

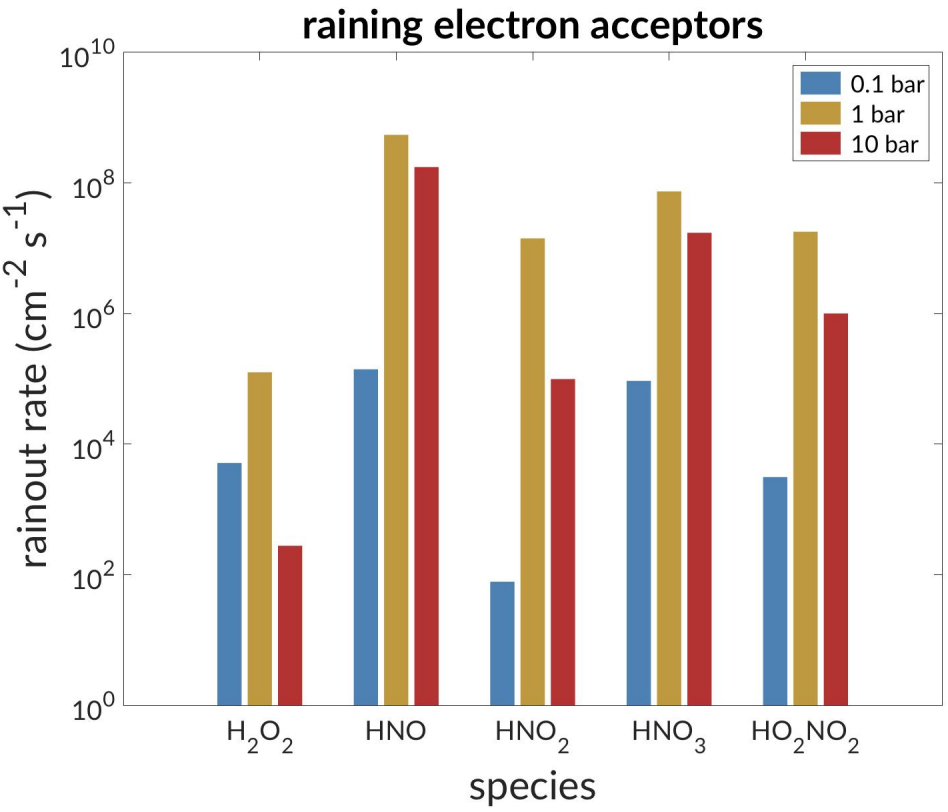

Fig. 5. The rainout rates of prospective electron acceptors for the emergence of life across all three atmospheric models. In every atmosphere tested, HNO is the dominant precipitate. For all species, the 1-bar pCO_2 case returns the maximum rainout rate.

The rainout rate of H_2O_2, another effective electron acceptor that is generated on early Earth, is quoted for comparison. In the 0.1-bar pCO_2 case, H_2O_2 makes up only 2% of the electron acceptors delivered from the atmosphere to the ocean. This fraction drops to 0.02% and 0.0001% in the 1-bar and 10-bar cases,

respectively, which is to be expected as the amount of CO_2 increases but the surface mixing ratio of H_2 remains constant. Although H_2O_2 should be considered as a possible electron acceptor for early metabolisms, it was by no means the dominantly available species.

pCO_2 (bar)	**0.1**	**1**	**10**
T_{surf} (K)	280.4	332.8	388.1
Lightning flash rate (flashes km^{-2} yr^{-1})	0.41	9.3	3.1
NO flux (molecules cm^{-2} s^{-1})	6.5×10^{6}	1.7×10^{9}	5.6×10^{8}
H2O2 rain (molecules cm^{-2} s^{-1})	5.1×10^{3}	1.3×10^{5}	2.8×10^{2}
HNO rain (molecules cm^{-2} s^{-1})	1.4×10^{5}	5.5×10^{8}	1.8×10^{8}
HNO_2 rain (molecules cm^{-2} s^{-1})	7.8×10^{1}	1.4×10^{7}	9.9×10^{4}
HNO_3 rain (molecules cm^{-2} s^{-1})	9.3×10^{4}	7.4×10^{7}	1.7×10^{7}
HO_2NO_2 rain (molecules cm^{-2} s^{-1})	3.1×10^{3}	1.8×10^{7}	1.0×10^{6}
Total NOx rain (molecules cm^{-2} s^{-1})	2.4×10^{5}	6.5×10^{8}	1.9×10^{8}
Time (Myr) to μM concentrations of NOx if no sinks	48	0.017	0.058
Equilibrium concentration (μM) of NOx assuming present-day hydrothermal circulation	8.7	2.4×10^{4}	7.2×10^{3}

Table 3. A summary of the results of the three cases: 0.1, 1, and 10 bars of CO_2. Surface temperatures and the lightning flash rates were calculated using the Generic LMDZ 3-D global climate model for early Earth. The NO fluxes were evaluated using data presented in **Fig. 2**. The rainout fluxes were calculated using the Caltech/JPL 1-D photochemical model. The equilibrium concentration was calculated using the simple box model discussed in the text and represented in **Fig. 6**.

Our models reveal that HNO_3 rainout is one of the primary sources of high-potential electron acceptors in the early ocean, eclipsing both HNO_2 and HO_2NO_2 rainout in all three cases. The normal pathway for generating HNO_3,

$NO_2 + OH + M \longrightarrow HNO_3 + M,$ (R1)

is stifled in the troposphere due to lack of OH. Although OH is being generated by water photolysis, it is also being consumed by the reaction

$CO + OH \longrightarrow CO_2 + H$ (R2)

at high rates due to the rapid photolysis of CO_2,

$CO_2 + h\nu \longrightarrow CO + O.$ (R3)

Thus, we have included the minor channel of $HO_2 + NO$ (Butkovskaya et al., 2007) in our photochemical model:

$HO_2 + NO \longrightarrow OH + NO_2$ major channel (R4a);

$HO_2 + NO + M \longrightarrow HNO_3 + M$ minor channel (R4b).

Though negligible when OH is plentiful and R1 is efficient, we find that this new pathway (R4b) dominates HNO_3 production on early Earth.

The measurements of the rate coefficient of reaction R4b (Butkovskaya et al., 2009, 2007, 2005) have not been reproduced by other groups. In their

evaluations, Sander et al. (2003) declined to make a recommendation for a preferred value. Recent experiments (Okumura, 2016, private communication) have indicated that the upper limit for the rate coefficient could be 2.5 times smaller than that reported in the previous work. Until further laboratory measurements are available, we warn that the production rate of HNO_3 in our models could be overestimated by a factor of ~3.

4. OCEANIC CONCENTRATIONS OF NOx

After raining out, HNO will yield nitrate and nitrite via the following aqueous reactions (Summers and Khare, 2007):

$$HNO \longrightarrow H^+ + NO^-$$

$$NO^- + NO \longrightarrow N_2O_2^-$$

$$N_2O_2^- + NO \longrightarrow N_3O_3^-$$

$$N_xO_x^- \longrightarrow NO_3^- + NO_2^- + N_2O.$$

HNO_3 and HNO_2 simply dissociate into H^+ and NO_3^- or NO_2^-, respectively. HO_2NO_2 will deoxygenate rapidly, producing nitrite:

$HOONO_2 \longrightarrow HOO^+ + NO_2^- \longrightarrow H^+ + O_2 + NO_2^-$.

If the ocean reservoir has no sink for nitrate or nitrite, and assuming that every dissolved HNO molecule eventually contributes a nitrate or nitrite, it would take 48, 0.017, and 0.058 Myr in the 0.1-, 1-, and 10-bar pCO_2 cases, respectively, to build up to μM concentrations in the Hadean ocean (taking the Hadean ocean volume to be 3×10^{18} m^3 in volume). The timescales for the 1- and 10-bar cases—merely blinks of an eye geologically speaking—reveal that a thick, CO_2-dominated Hadean atmosphere was quite efficient at pumping nitrogen oxides into the ocean. Even the rainout in the 0.1-bar case is not insignificant. However, to better address the possibility that nitrate played an important role as an electron acceptor for denitrifying methanotrophic acetogenesis, we should consider other nitrate loss mechanisms (aside from those directly involved in this metabolic pathway), and solve for the equilibrium concentration of nitrate in the Hadean ocean.

NO_3^- is a primary nutrient for life in today's oceans; it is consumed as a source of nitrogen by some organisms and respired (denitrified to N_2) by others. However, these powerful biological sinks were, of course, completely absent before the emergence of life. Instead, we must examine abiotic processes to characterize the most effective nitrate sinks.

The Hadean ocean is expected to have had dissolved Fe^{2+}, which is known to originate at hydrothermal systems, and which can be oxidized to Fe^{3+}. However, we consider Fe^{2+} to be inefficient at reducing nitrate or nitrite, because on present-

day Earth, where there is an abundance of nitrate and nitrite, dissolved ferrous iron is able to traverse thousands of kilometers from its origin at hydrothermal vent sites to scientific sampling stations without trouble (Fitzsimmons et al., 2014).

Summers (2005) showed experimentally that FeS suspensions can reduce nitrite to ammonium in Hadean ocean environments. Nitrate can also be reduced to ammonium, but at a significantly lower yield. Summers (2005) could not reduce nitrate to ammonium at pH > 6.9, indicating that nitrate is probably not reduced by iron sulfide in great amounts by this process at alkaline hydrothermal vents. Furthermore, nitrate is not readily reduced to ammonium in the presence of other species like Cl^- and SO_4^{-2}. We expect such anions to be dissolved in the Hadean ocean, making nitrate reduction by FeS insignificant.

Aqueous photochemistry at the ocean surface is capable of converting nitrate into nitrite and vice versa (Mack and Bolton, 1999), but because both species can serve as electron acceptors, this would not present a problem for the emergence of life. Because this photochemistry only affects a tiny fraction of the ocean, the nitrate lost to nitrite in this manner, which can then be reduced by FeS, is negligible in the present context.

Thus, we consider the dominant NOx loss mechanism to be extreme heating (~400 °C) as ocean water cycles through acidic hydrothermal vents. At such high temperatures, nitrate and nitrite would be reduced back to N_2 by iron minerals within the crust. There may also be some reduction of nitrate in the water cycling by moderate-temperature, serpentinization-driven alkaline springs, though the

product in this case is likely to be ammonia, thus merely adding to that entity at alkaline vents (Gordon et al., 2013).

We construct a simple box model to ascertain the equilibrium nitrate concentration (Fig. 6). Assuming 100% destruction of NOx at black-smoker temperatures, the equilibrium number concentration of NOx is

$$C_{\mathrm{NOx}} = \frac{f_{\mathrm{atm}} A_{\oplus} \tau_{\mathrm{HTV}}}{V_{\mathrm{ocean}}},$$

where f_{atm} is the NOx flux from the atmosphere (molecules $\mathrm{cm^{-2}\ s^{-1}}$), $A_{\oplus}$ is the surface area of Earth (5.1×10^{18} $\mathrm{cm^3}$), τ_{HTV} is the timescale for cycling through high-temperature vents, and V_{ocean} is the volume of the Hadean ocean (~3×10^{18} $\mathrm{m^3}$). Because $\tau_{\mathrm{HTV}} = V_{\mathrm{ocean}}/F_{\mathrm{HTV}}$, where F_{HTV} is the mass flux of water through high-temperature hydrothermal vents,

$$C_{\mathrm{NOx}} = \frac{f_{\mathrm{atm}} A_{\oplus}}{F_{\mathrm{HTV}}}.$$

According to Nielsen et al., 2006, the current water mass flux from high-temperature vents is 7.2×10^{12} kg $\mathrm{yr^{-1}}$. Using this present-day value and $f_{\mathrm{atm}} \sim 6.5 \times 10^8$ molecules $\mathrm{cm^{-2}\ s^{-1}}$ (as in the 1-bar case), then $C_{\mathrm{NOx}} =$ 24 mM. Acidic vents were more prevalent in the Hadean, though by what degree is still unknown. However, unless the water flux through high-temperature vents was thousands of times as great as today, the equilibrium nitrate concentration would still exceed 1 μM.

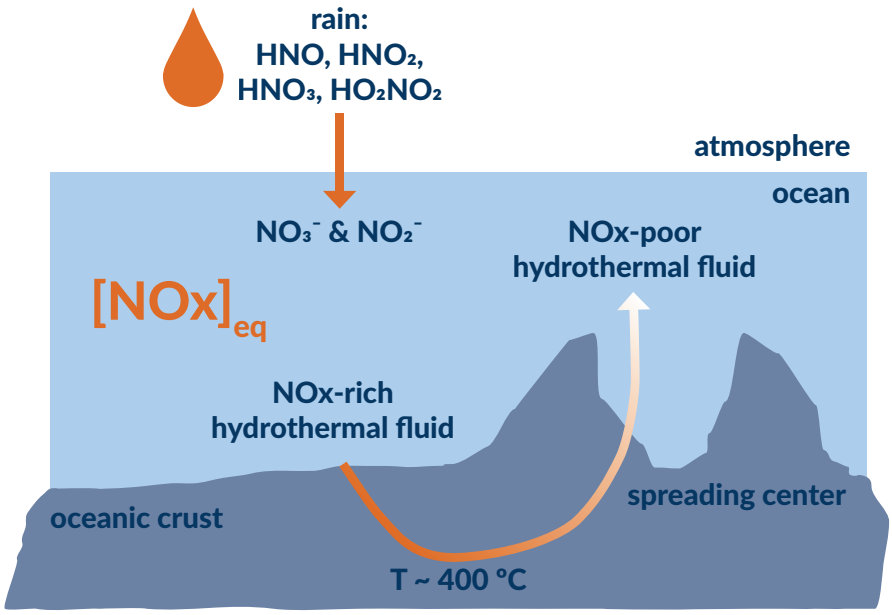

Fig. 6. A simple box model for calculating the equilibrium concentration of nitrate and nitrite in the Hadean ocean. We assume that the primary source is acid rain from the atmosphere and that the dominant sink is removal by extreme heating at high-temperature hydrothermal sites.

5. CONCLUSION

NOx are thought to be needed as high-potential electron acceptors for the emergence of metabolism at submarine alkaline hydrothermal vents. NOx are created in early Earth's CO_2–N_2 atmosphere, but the atmospheric pressure during the Hadean is uncertain and likely varied widely. We have demonstrated, using atmospheric models supported by data, that there was a prevalence of NOx produced in the Hadean atmosphere for a large range of pCO_2. This NOx rained out into the Hadean ocean primarily as HNO, which reacted to form nitrate and nitrite in solution. Although the 10-bar pCO_2 case probably only applies to the first few 10s Myr of Earth's history, it still produced significant amounts of NOx. As

the pCO_2 settled around 0.1–1 bar for the long-term, copious NOx was also being delivered to the Hadean ocean. If the water flux through high-temperature hydrothermal vents was not more than thousands of times what it is today, the steady-state nitrate concentration would be micromolar, supplying onsite electron acceptors and a potential amino source at the emergence of life.

ACKNOWLEDGEMENTS

This research was supported in part an NAI Virtual Planetary Laboratory grant from the University of Washington to the Jet Propulsion Laboratory and California Institute of Technology. B.C. acknowledges support from an appointment to the NASA Postdoctoral Program, administered by Universities Space Research Association. MJR's research was supported by the National Aeronautics and Space Administration, through the NASA Astrobiology Institute under cooperative agreement issued through the Science Mission directorate; No. NNH13ZDA017C (Icy Worlds) at the Jet Propulsion Laboratory.

CONCLUSIONS

ASTROBIOLOGICAL IMPLICATIONS

The three worlds—Titan, Pluto, and Earth—are not only intriguing from an atmospheric photochemistry point of view, but also from an astrobiological vantage.

Titan is Nature's organosynthesis factory. The photochemical production of organics on Titan is reliant on an autocatalytic cycle in its atmosphere called *photosensitized dissociation*. As described in Chapter 1, methane photolysis leads to the creation of acetylene, which itself can be photolyzed to create ethynyl radicals, which attack methane to create more acetylene via a bimolecular reaction. Thus, there is a positive feedback loop spurring the destruction of CH_4, the creation of C_2H_2, and the onset of other photochemical pathways leading up to hydrocarbon aerosols.

It stirs the imagination to note the parallels between the autocatalytic nature of biosynthesis in life and the autocatalytic nature of organosynthesis in Titan's atmosphere. If carbon-based life were to exist on Titan's alien shores, it might utilize some kind of photosynthetic pathway akin to the abiotic production of organics above. Perhaps the two are not causally independent.

So many aspects of Titan remain to be solved. One of the biggest mysteries is the origin of Titan's atmospheric methane. It is a distinct possibility that Titan's current methane-rich state is abnormal and that Titan's distant past featured distinctively colder conditions, i.e. Snowball Titan. (Yes, Titan is already a Snowball in its present state, but I appropriated the name from terrestrial science, where "Snowball Earth" is used to describe a radically colder global climate state from the one we currently enjoy.) In the future, after all of the methane in Titan's

atmosphere is irreversibly converted into higher-order hydrocarbons, these conditions will return.

We find that on Snowball Titan, the photochemical creation of nitriles (molecules containing a C–N bond) relative to hydrocarbons is quite enhanced. Snowball Titan illustrates that while autocatalytic systems are powerful, they can also be fragile. If you remove just a single step in the positive feedback loop that drives hydrocarbon production on Titan, the entire mechanism collapses, allowing nitriles to dominate. Life, too, is a high-wire act. Remove an essential ingredient from our diets or stifle a critical enzyme, and our metabolisms collapse.

One nitrile of increased prevalence on Snowball Titan is acrylonitrile (C_2H_3CN), the proposed building block for *asotozomes*—theoretical membranes that have similar physical properties in methane–ethane solutions as phospholipid membranes have in aqueous solution. Acrylonitrile has been detected in Titan's atmosphere, and the downward flux of acrylonitrile should be enough to fill one cubic centimeter of Titan lake material with 3×10^7 azotosomes—spherical vessels that could serve as membranes for titanian microbiota (Palmer et al., 2017; Stevenson et al., 2015). At the time of the Snowball Titan paper's publication, acrylonitrile had little significance, as neither the theoretical work that modeled asotozomes nor the observational work that detected acrylonitrile on Titan had been performed. Hence, it was especially pleasing to revisit our Snowball Titan paper and see acrylonitrile as a major photochemical prediction.

Nitriles in general would also be useful to life on Titan from a reduction/oxidation point of view. Although not quite as powerful as oxygen,

nitrogen is a relatively strong electron acceptor. So a nitrile-dominated world would set up ripe redox gradients that putative biology could exploit. If the Snowball Titan story is true, this means that once Titan escaped its formerly frigid state and produced liquid hydrocarbon seas like we see today, a preexisting array of nitrogen-bearing compounds were lying in wait to be used. For this reason, Snowball Titan may make life on Titan a more likely possibility.

Of course, nothing resembling life may exist on Titan's surface. At the very least, the Snowball Titan idea offers a narrative that helps explain the current budget of organics on Titan's surface, reminds us to consider radically different climates over geologic history, and gives us a prediction that a future Titan mission—like the octocopter concept Dragonfly—could test. Currently, Titan's dune material lacks characterization: to Cassini's payload, it was spectroscopically indistinct. If in the future Titan's dune material is determined to contain a plethora of nitrile species rather than hydrocarbons, that would be a powerful point in favor of an ancient Snowball Titan epoch.

Pluto copies Titan's flavor of organosynthesis: its nitrogen-dominated atmosphere with minor amounts of methane is impinged upon by UV radiation and energetic particles to create organics that eventually lead to fractal aggregate aerosols. However, Pluto's is far too frigid for any liquid medium to persist on its surface. And although some evidence points to Pluto being an ocean world—that is, it might have a slowly freezing subsurface ocean of liquid water (Nimmo et al., 2016; Robuchon and Nimmo, 2011)—it is a far less promising habitat than, say, Europa or Enceladus.

The best connection between Pluto and life might stem from the "Is Pluto a planet?" debate. Deciding what to call a planet and deciding what to call life are similar in their pedagogic value. Categorizing things into planets and non-planets helps us interpret the architecture of the Solar System. It helps us understand *why* certain structures are the way they are.

The International Astronomical Union's (IAU) definition of a planet is poorly worded. It states that a planet

1) is in orbit around the Sun,
2) has sufficient mass to assume hydrostatic equilibrium, and
3) has "cleared the neighborhood" around its orbit.

Following the exact words of this definition, exoplanets, which orbit other stars, are not planets. But exoplanets are clearly planets. And one cannot overstate the befuddling vagueness of "cleared the neighborhood," which threatens to allow Jupiter's Trojan asteroids to disqualify our most obvious planet from planethood.

Yet while the exact words of the IAU's definition are misleading, the spirit of the words is not. Planets should: 1) be gravitationally bound to stars; 2) gravitationally determine their own shape; 3) gravitationally dominate their orbital space. Gravity, gravity, gravity.

Pluto is not a planet because it does not fulfill the spirit of the third requirement. Pluto shares its orbital space with the other members of the Kuiper belt—a vast ring of debris similar to the asteroid belt, but icier and beyond the orbit

of Neptune. Just as Jupiter's disruptive influence never allowed asteroids the chance to coagulate into a single body, i.e. a bona fide planet, Neptune's presence kept Kuiper belt objects (KBOs) in dynamical disarray.

It's true that Jupiter shares its orbit with the Trojan asteroids, but the Trojans only occupy Jupiter's Lagrange points because Jupiter's gravity affords them this existence. Jupiter is the boss; the Trojans march to the beat of its drum. In contrast, Pluto and all of the other Plutinos, KBOs that are locked in a 3:2 orbital resonance with Neptune, are being *bossed around* by Neptune's gravity. The other KBOs don't give a comet's tail that Pluto is among them. It's Neptune who's setting the pace.

Supporters of Pluto's planethood often decry the orbital dominance criterion by stating that if the Earth were suddenly moved to the asteroid belt, it wouldn't be considered a planet anymore. But they're missing the point. Instead of *hypothetically* moving Earth into the asteroid belt, one should ask instead why a *real* Earth-mass planet didn't form in that region. Again, it's gravity's fault.

Gravity is the force that guides the architectural evolution of planetary systems. It dictates that some objects will evolve to dominate their orbital space, and that others—of perhaps equal surface, atmospheric, and structural interest—will not. That some objects are planets and others are not is a real, observable difference. And deciding what to call a planet and what not to call a planet helps us understand the history of the Solar System as shaped by the fundamental force of gravity.

We define planets by what they do: Pluto may *look* like a planet, but it doesn't *act* like one, at least not in the arena of planet system architecture. Similarly, Pluto has complex organics. But being made of complex organics *alone* does not make you alive. Like planetary system architecture, life is state of complexity resultant from the laws of nature. Instead of asking what life is, we should ask what it does. The lesson from Pluto: Life is a verb, not a noun.

Understanding what life *does* gives us clues as to how life might *begin* on any wet, rocky world. So what does life do?

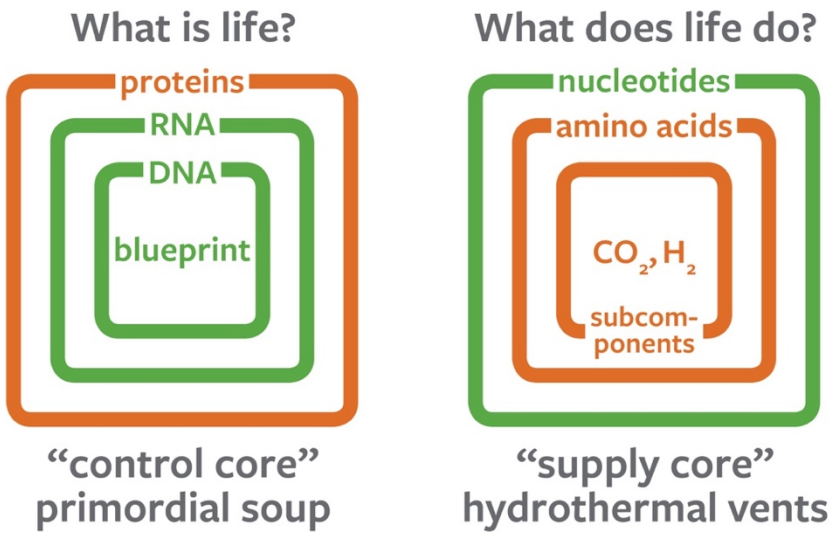

Fig. 1. (After Cairns-Smith, 1985) Two fundamentally different ways of viewing life: "What is life?" vs. "What does life do?" **(a)** The former emphasizes the information carried in nucleic acids and suggests an origin story that begins with the creation of the first self-replicating polymer. In this model, metabolism follows replication once the replicator learns to also catalyze the formation of other useful organic molecules, like proteins. **(b)** The latter emphasizes metabolism, which is based upon the fundamental redox disequilibrium of terrestrial planets, and suggests an origin story that begins with the first metabolic engine. In this model, information-carrying molecules emerged from a proto-metabolic network.

Life as we know it can be described as an organometallic dissipative structure that liberates free energy and raises the entropy of the universe by resolving redox gradients in its environment. Life achieves its ordered state by coupling endergonic processes, such as the synthesis of far-from-equilibrium organic structures, to highly exergonic processes, e.g. the dissipation of redox gradients. The choice of asking "What does life do?" is a paradigm shift that places metabolism at the core (Fig. 1).

It's common knowledge that ATP is the energy currency of life—its usage is universal. Perhaps the more enlightening fact, however, is that the peculiar process that everything uses to make ATP is universal, too. Although life ultimately derives its free energy from redox disequilibria, it transduces that free energy twice—first into a proton (H^+) gradient, and then into ATP (Fig 2.).

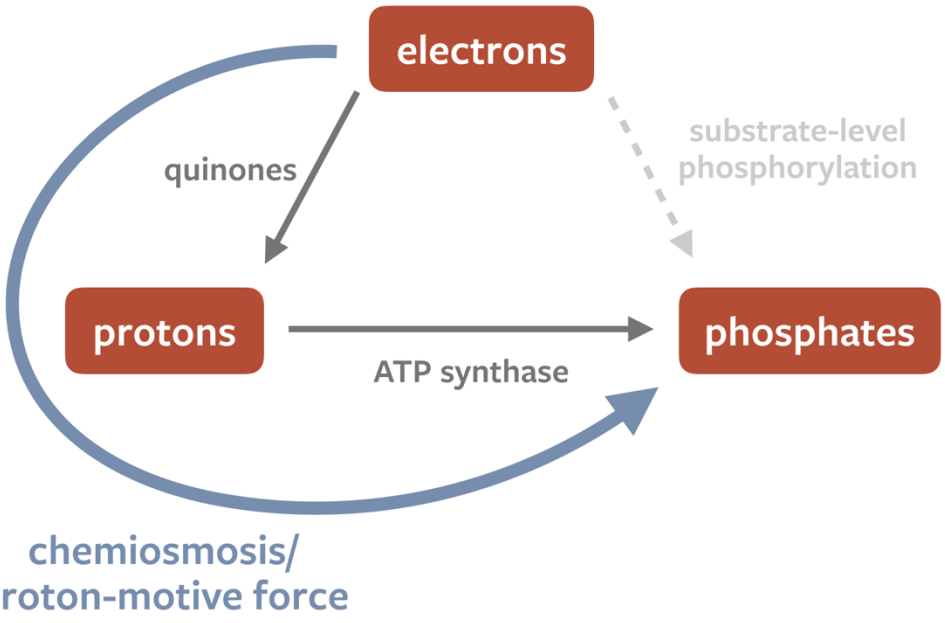

Fig. 2. (After Smith and Morowitz, 2016) The cellular energy triangle. Biology utilizes three energy buses in its metabolism: electrons, protons, and phosphates. Electrons release free energy via redox reactions, which is

transduced into a proton gradient. The proton gradient drives ATP synthase, storing free energy in a disequilibrium between ATP and its hydrolysis products ADP + P_i. Modern life can also perform substrate-level phosphorylation (SLP), directly harnessing the free energy from redox reactions into ATP. However, SLP is never the sole source of ATP in any organism and is not the primary source of ATP synthesis in most organisms.

The electron transport chain in cell membranes uses the liberated free energy from redox reactions to pump protons from one side of the membrane to the other. These protons then stream back across the membrane through a molecular machine called ATP synthase. *Chemiosmosis* is the process of using a flow of protons (H^+) to crank ATP synthase, binding adenosine *di*phosphate (ADP) to phosphate (P_i) to make ATP.

Among origin-of-life theories, only the alkaline hydrothermal vent (AHV) hypothesis offers a compelling explanation for the universality of chemiosmosis. The pH gradient at Hadean alkaline hydrothermal vents provides a natural proton-motive force between high-H^+ oceanic fluid and the low-H^+ vent fluid. If this proton-motive force could be coupled to phosphorylation at the emergence of life, e.g. by some primitive inorganic pyrophosphatase (Mike Russell at JPL suspects green rust, though this has yet to be confirmed experimentally), one could argue that modern biology is attempting to recreate its initial conditions by pumping protons across a membrane only to let them return.

Hadean AHVs would not just host proton disequilibria but also redox disequilibria. Found a few tens of kilometers off of oceanic spreading ridges, alkaline vents are driven by *serpentinization*, a process in which water interacts with

ultramafic rocks called peridotites. Serpentinization refers to a class of water–rock reactions in which H_2O oxidizes olivine. The particular reaction involving fayalite (Fe_2SiO_4), the iron end-member of olivine, produces magnetite (Fe_3O_4), aqueous silica (SiO_2), and pure hydrogen gas (H_2):

$$3\ Fe_2SiO_4 + 2\ H_2O \longrightarrow 2\ Fe_3O_4 + 3\ SiO_2 + 2\ H_2.$$

Upon returning to the ocean, this water is now laden with H_2 and is far more alkaline (pH ~ 11). The difference in pH between hydrothermal fluids and the ambient ocean results in the precipitation of hydrothermal chimneys made of aragonite ($CaCO_3$) and brucite ($Mg[OH]_2$), some up to 60 meters tall (Fig. 3).

Fig. 3. (Credit: Kelley, U of Washington, IFE, URI-IAO, NOAA) Image of a hydrothermal chimney at the Lost City hydrothermal field. Today, magma-driven vents host thick ecosystems of macrofuana as well as microbiota, while serpentinization-driven vents support diverse microbial communities.

In the Hadean, submarine serpentinizing systems would inject their H_2-rich, high-pH water into a much different ocean. Overlain by a thick CO_2 atmosphere, the Hadean ocean would have had a high concentration of dissolved CO_2, making it slightly acidic (pH ~ 5). Thus, alkaline hydrothermal vents were extreme focusing centers for two kinds of disequilibria: a redox gradient between pure H_2 and CO_2 as well as a pH gradient of ~6 log units.

Serpentinization is an exothermic reaction, so there would have also been a temperature gradient between the interior and the exterior of each hydrothermal mound. This temperature gradient would result in a process known as *thermophoresis*, which served to concentrate large organic molecules in pore spaces while allowing smaller waste products of a nascent metabolic network, like acetate, to leave the system (Herschy et al., 2014).

Furthermore, the Hadean ocean was anoxic, so the vent walls would contain precipitates of catalytic iron-sulfur minerals. Many of these minerals, such as mackinawite, greigite, and violarite, share remarkably similar chemical structures to the active sites of metalloenzymes widespread in biology today, including those that help fix CO_2 and utilize H_2 (Fig. 4) (Nitschke et al., 2013). Another mineral, fougèrite ($[Fe^{2+}_4Fe^{3+}_2(OH)_{12}][CO_3]\cdot 3H_2O$), commonly called *green rust*, has the ability to reduce nitrate (NO_3^-) to ammonia (NH_3), which is useful for the amination of the first amino acids (Hansen et al., 2001; Trolard & Bourrié, 2012). Green rust is a double-layered hydroxide; the interstices between its layers present a water-poor environment that can concentrate organics and lead to synthesis.

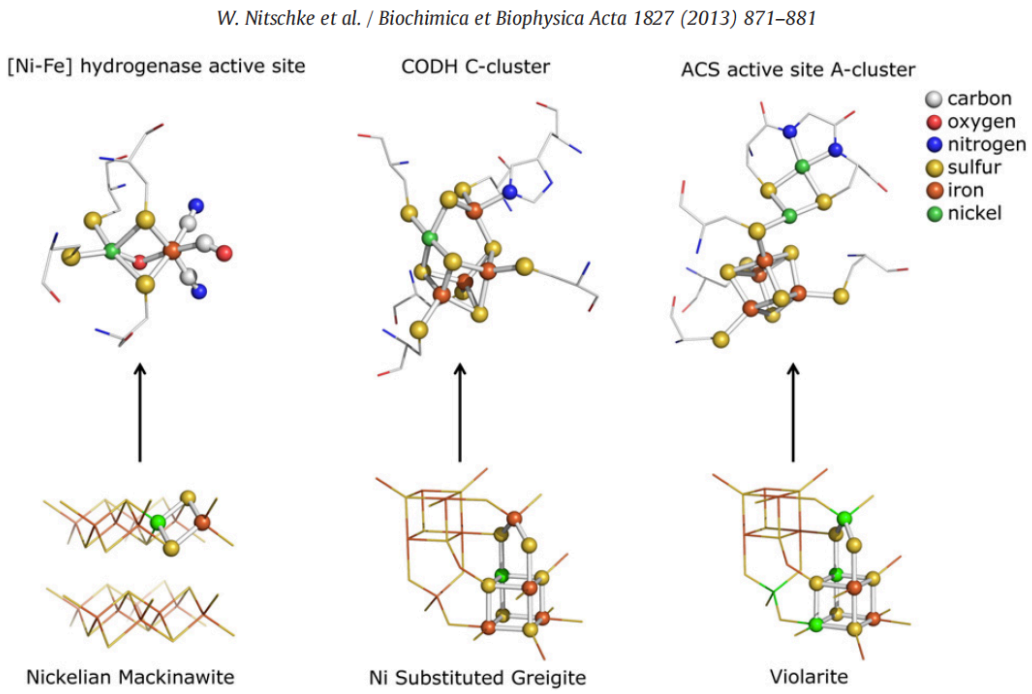

Fig. 4. (From Nitschke et al., 2013) The similarity between the active sites of melloenzymes in biology and the structures of naturally occurring minerals in Hadean hydrothermal vent walls.

The prevalence of inorganic catalysts in biological enzymes may be no mistake. These specific structures—or their evolutionary predecessors, at least—could have been incorporated from the walls of ancient hydrothermal mounds. Such minerals were the art trouvé of life.

Thus, Hadean hydrothermal mounds were comprised of a porous maze of mineral vesicles ideal for creating the first biologically relevant organics, concentrating organic monomers, and catalyzing their polymerization.

My work in Chapter 3 on quantifying the delivery of NOx to the Hadean oceans is crucial to the AHV hypothesis for the emergence of life. Laboratory

studies have shown that although there is a large thermodynamic disequilibrium between H_2 and CO_2, they are highly unreactive in vent-like settings due to a large kinetic barrier. Carbon dioxide, in particular, is a relatively stable molecule. In order to be coerced into participating in redox reactions, CO_2 must be activated by an electron forced upon it, which is an endergonic process. Biology today uses a trick called *electron bifurcation* to overcome similar energetic barriers (Peters et al., 2016). In electron bifurcation, an electron donor donates two electrons simultaneously: one in an endergonic fashion (i.e. to activate CO_2) and the other in an exergonic fashion (to a high-potential electron acceptor). This double transfer can occur so long as the net reaction is exergonic. It just so happens that molybdenum, a transition metal that would have been supplied at Hadean alkaline vents at ~100 nmol/l, is used in present-day bioenergetics to make two-electron transfers (Nitschke et al., 2013). Molybdenum at AHVs could have been the initial catalyst that drove a CO_2–H_2-consuming metabolic engine into existence. Thus, the AHV hypothesis hinges on a high-potential electron acceptor for molybdenum.

To summarize, alkaline hydrothermal vents are promising sites for the emergence of life because:

1) the redox gradient between serpentinization-derived H_2 and dissolved CO_2 from the Hadean atmosphere, sparked by NOx delivered by lightning and photochemistry, provides free energy
2) the resulting reaction between H_2 and CO_2, along with the incorporation of fixed nitrogen from NOx species, creates organics

3) the pH gradient between hydrothermal fluid and the acidic carbonic ocean provides a natural proton-motive force
4) the presence of mineral catalysts help with the synthesis and polymerization of the first biomolecules
5) the temperature gradient results in thermophoresis, which helps concentrate larger organics and expel metabolic waste
6) the latest phylogenetic evidence indicates that LUCA was a thermophile that consumed H_2 and CO_2

In this thesis, we have built a new *perspective* on life—that life is an autocatalytic dissipative structure that serves as a conduit for electron flow through organometallic metabolic networks. The result is a startling realization that if similar situations existed on other worlds—and why should Earth be special?—then we should expect that the universe is littered with wet, rocky worlds teeming with life.

This is not a conclusion. It is a *hypothesis*. Carl Sagan would say it is an extraordinary claim that that requires extraordinary evidence.

The evidence—either for or against—will come from exploration. We must journey to other worlds and train our telescopes on those that are, for the moment, still beyond our grasp, ever asking about the possibility of things like us. In the next few years and decades, we will begin to characterize the atmospheres of countless terrestrial exoplanets. We will sample the oceans of Europa and Enceladus, where alkaline hydrothermal structures may exist. And we will learn more about the

earliest life on Earth and hunt for ancient life on Mars. But *now*, more than ever, is the time to hypothesize about life. As we reach out beyond the cosmic shore, we will either find life, or we will not. In either outcome, if we dare to hypothesize, then we will truly understand our place in the cosmos.

REFERENCES

Ackerman, A.S., Marley, M.S., 2001. Precipitating Condensation Clouds in Substellar Atmospheres. Astrophys. J. 556, 872–884. doi:10.1086/321540

Airapetian, V.S., Glocer, A., Gronoff, G., Hébrard, E., Danchi, W., 2016. Prebiotic chemistry and atmospheric warming of early Earth by an active young Sun. Nat. Geosci. 1–5. doi:10.1038/ngeo2719

Allen, M., Yung, Y.L., Waters, J.W., 1981. Vertical Transport and Photochemistry in the Terrestrial Mesosphere and Lower Thermosphere (50-120 km). J. Geophys. Res. 86, 3617–3627. doi:10.1029/JA086iA05p03617

Bianchi, A., Giorgi, C., Ruzza, P., Toniolo, C., Milner-White, E.J., 2012. A synthetic hexapeptide designed to resemble a proteinaceous p-loop nest is shown to bind inorganic phosphate. Proteins Struct. Funct. Bioinforma. 80, 1418–1424. doi:10.1002/prot.24038

Branscomb, E., Russell, M.J., 2013. Turnstiles and bifurcators: The disequilibrium converting engines that put metabolism on the road. Biochim. Biophys. Acta - Bioenerg. 1827, 62–78. doi:10.1016/j.bbabio.2012.10.003

Butkovskaya, N., Kukui, A., Bras, G. Le, 2007. HNO3 Forming Channel of the HO2 + NO Reaction as a Function of Pressure and Temperature in the Ranges of 72–600 Torr and 223–323 K. J. Phys. Chem. A 111, 9047–9053.

Butkovskaya, N., Rayez, J., Kukui, A., Bras, G. Le, 2009. Water Vapor Effect on the HNO3 Yield in the HO2 + NO Reaction: Experimental and Theoretical Evidence. J. Phys. Chem. A 113, 11327–11342.

Butkovskaya, N.I., Kukui, A., Pouvesle, N., Bras, G. Le, 2005. Formation of Nitric Acid in the Gas-Phase HO2 + NO Reaction: Effects of Temperature and Water Vapor. J. Phys. Chem. A 109, 6509–6520. doi:10.1021/jp051534v

Cairns-Smith, A.G., 1985. Seven Clues to the Origin of Life. Cambridge University Press, Cambridge.

Charnay, B., Forget, F., Tobie, G., Sotin, C., Wordsworth, R., 2014. Titan's past and future: 3D modeling of a pure nitrogen atmosphere and geological implications. Icarus 241, 269–279. doi:10.1016/j.icarus.2014.07.009

Charnay, B., Forget, F., Wordsworth, R., Leconte, J., Millour, E., Codron, F., Spiga, A., 2013. Exploring the faint young Sun problem and the possible climates of the Archean Earth with a 3-D GCM. J. Geophys. Res. Atmos. 118, 10,414-10,431. doi:10.1002/jgrd.50808

Choi, Y., Kim, J., Eidering, A., Osterman, G., Yung, Y.L., Gu, Y., Liou, K.N., 2009. Lightning and anthropogenic NOx sources over the United States and the western North Atlantic Ocean: Impact on OLR and radiative effects. Geophys. Res. Lett. 36, 1–5. doi:10.1029/2009GL039381

Claire, M.W., Sheets, J., Cohen, M., Ribas, I., Meadows, V.S., Catling, D.C., 2012. THE EVOLUTION OF SOLAR FLUX FROM 0.1 nm TO 160 μm: QUANTITATIVE ESTIMATES FOR PLANETARY STUDIES. Astrophys. J. 757, 95. doi:10.1088/0004-637X/757/1/95

Ducluzeau, A.L., van Lis, R., Duval, S., Schoepp-Cothenet, B., Russell, M.J.,

Nitschke, W., 2009. Was nitric oxide the first deep electron sink? Trends Biochem. Sci. 34, 9–15. doi:10.1016/j.tibs.2008.10.005

Fitzsimmons, J.N., Boyle, E.A., Jenkins, W.J., 2014. Distal transport of dissolved hydrothermal iron in the deep South Pacific Ocean 111, 16654–16661. doi:10.1073/pnas.1418778111

Forget, F., Wordsworth, R., Millour, E., Madeleine, J.B., Kerber, L., Leconte, J., Marcq, E., Haberle, R.M., 2013. 3D modelling of the early martian climate under a denser CO2 atmosphere: Temperatures and CO2 ice clouds. Icarus 222, 81–99. doi:10.1016/j.icarus.2012.10.019

Gao, P., Fan, S., Wong, M.L., Liang, M.-C., Shia, R.-L., Kammer, J.A., Summers, M.E., Gladstone, G.R., Young, L.A., Olkin, C.B., Ennico, K., Weaver, H.A., Stern, S.A., Yung, Y.L., Science Team, N.H., 2016. Microphysics of Pluto's Photochemical Haze and Comparison to New Horizons Observations. Icarus.

Gao, P., Fan, S., Wong, M.L., Liang, M., Shia, R., Kammer, J.A., Yung, Y.L., Summers, M.E., Gladstone, G.R., Young, L.A., Olkin, C.B., Ennico, K., Weaver, H.A., Stern, S.A., 2017. Constraints on the microphysics of Pluto's photochemical haze from New Horizons observations. Icarus 287, 116–123. doi:10.1016/j.icarus.2016.09.030

Génin, J.M.R., Abdelmoula, M., Aïssa, R., Ruby, C., 2005. Ordering in FeII-III hydroxysalt green rusts from XRD and Mössbauer analysis (chloride, carbonate, sulphate, oxalate...); about the structure of hydrotalcite-like compounds. Hyperfine Interact. 166, 391–396. doi:10.1007/s10751-006-

9298-1

Génin, J.M.R., Ruby, C., Géhin, A., Refait, P., 2006. Synthesis of green rusts by oxidation of Fe(OH)2, their products of oxidation and reduction of ferric oxyhydroxides; Eh-pH Pourbaix diagrams. Comptes Rendus - Geosci. 338, 433–446. doi:10.1016/j.crte.2006.04.004

Gladstone, G.R., Pryor, W.R., Alan Stern, S., 2015. Lyα@Pluto. Icarus 246, 279–284. doi:10.1016/j.icarus.2014.04.016

Gladstone, G.R., Stern, S.A., Ennico, K., Olkin, C.B., Weaver, H.A., Young, L.A., Summers, M.E., Strobel, D.F., Hinson, D.P., Kammer, J.A., Parker, A.H., Steffl, A.J., Linscott, I.R., Parker, J.W., Cheng, A.F., Slater, D.C., Versteeg, M.H., Greathouse, T.K., Retherford, K.D., Throop, H., Cunningham, N.J., Woods, W.W., Singer, K.N., Tsang, C.C.C., Schindhelm, E., Lisse, C.M., Wong, M.L., Yung, Y.L., Zhu, X., Curdt, W., Lavvas, P., Young, E.F., Tyler, G.L., 2016. The atmosphere of Pluto as observed by New Horizons. Science (80-.). 351, 1280. doi:10.1126/science.aad8866

Gordon, A.D., Smirnov, A., Shumlas, S.L., Singireddy, S., DeCesare, M., Schoonen, M.A.A., Strongin, D.R., 2013. Reduction of Nitrite and Nitrate on Nano-dimensioned FeS. Orig. Life Evol. Biosph. 43, 305–322. doi:10.1007/s11084-013-9343-4

Hampson, R.F.J., Garvin, D., 1977. Reaction Rate and Photochemical Data for Atmospheric Chemistry - 1977. Natl. Bur. Stand. Spec. Publ. 513.

Helz, G.R., Erickson, B.E., Vorlicek, T.P., 2014. Stabilities of thiomolybdate complexes of iron; implications for retention of essential trace elements (Fe, Cu, Mo) in sulfidic waters. Metallomics 6, 1131–40. doi:10.1039/c3mt00217a

Herschy, B., Whicher, A., Camprubi, E., Watson, C., Dartnell, L., Ward, J., Evans, J.R.G., Lane, N., 2014. An Origin-of-Life Reactor to Simulate Alkaline Hydrothermal Vents. J. Mol. Evol. 79, 213–227. doi:10.1007/s00239-014-9658-4

Huber, C., Wächtershäuser, G., 2003. Primordial reductive amination revisited. Tetrahedron Lett. 44, 1695–1697. doi:10.1016/S0040-4039(02)02863-0

Huber, C., Wächtershäuser, G., 1997. Activated acetic acid by carbon fixation on (Fe, Ni) S under primordial conditions. Science (80-.). 276, 245–247. doi:10.1126/science.276.5310.245

Kasting, J.F., 1993. Earth's early atmosphere. Science (80-.). 259, 920–926.

Kasting, J.F., Walker, J.C.G., 1981. Limits on oxygen concentration in the prebiological atmosphere and the rate of abiotic fixation of nitrogen. J. Geophys. Res. 86, 1147. doi:10.1029/JC086iC02p01147

Kawamura, K., Takeya, H., Kushibe, T., Koizumi, Y., 2011. Mineral-enhanced hydrothermal oligopeptide formation at the second time scale. Astrobiology 11, 461–9. doi:10.1089/ast.2011.0620

Kelley, D.S., Karson, J. a, Blackman, D.K., Früh-Green, G.L., Butterfield, D. a, Lilley, M.D., Olson, E.J., Schrenk, M.O., Roe, K.K., Lebon, G.T., Rivizzigno, P., 2001. An off-axis hydrothermal vent field near the Mid-

Atlantic Ridge at 30 degrees N. Nature 412, 145–149. doi:10.1038/35084000

Kirschvink, J.L., Gaidos, E.J., Bertani, L.E., Beukes, N.J., Gutzmer, J., Maepa, L.N., Steinberger, R.E., 2000. Paleoproterozoic snowball Earth: Extreme climatic and geochemical global change and its biological consequences. Proc. Natl. Acad. Sci. 97, 1400–1405.

Kopp, R.E., Kirschvink, J.L., Hilburn, I.A., Nash, C.Z., 2005. The Paleoproterozoic snowball Earth: A climate disaster triggered by the evolution of oxygenic photosynthesis. Proc. Natl. Acad. Sci. 102, 11131–11136.

Krasnopolsky, V.A., 2009. A photochemical model of Titan's atmosphere and ionosphere. Icarus 201, 226–256. doi:10.1016/j.icarus.2008.12.038

Krasnopolsky, V.A., Cruikshank, D.P., 1999. Photochemistry of Pluto's atmosphere and ionosphere near perihelion. J. Geophys. Res. 104, 21,979-21,996.

Lara, L.M., Lellouch, E., López-Moreno, J.J., Rodrigo, R., 1996. Vertical distribution of Titan's atmospheric neutral constituents. J. Geophys. Res. 101, 23261. doi:10.1029/96JE02036

Lavvas, P., Griffith, C.A., Yelle, R. V., 2011. Condensation in Titan's atmosphere at the Huygens landing site. Icarus 215, 732–750. doi:10.1016/j.icarus.2011.06.040

Le Gall, A., Rodriguez, S., Garcia, A., Radebaugh, J., Lorenz, R.D., Lopes, R.M.C., Hayes, A., Reflet, E., 2012. Titan's Dunes by the Numbers, in:

Third International Planetary Dunes Workshop. Flagstaff, AZ, USA.

Lellouch, E., Bergh, C. De, Sicardy, B., Käufl, H.U., Smette, A., 2011. High resolution spectroscopy of Pluto ' s atmosphere : detection of the 2 . 3 μ m CH 4 bands and evidence for carbon monoxide 4, 8–11.

Lellouch, E., Gurwell, M., Butler, B., Fouchet, T., Lavvas, P., Strobel, D.F., Sicardy, B., Moullet, A., Moreno, R., Bockelée-morvan, D., Biver, N., Young, L., Lis, D., Stansberry, J., Stern, A., Weaver, H., Young, E., Zhu, X., Boissier, J., 2017. Detection of CO and HCN in Pluto' s atmosphere with ALMA. Icarus 286, 289–307. doi:10.1016/j.icarus.2016.10.013

Lellouch, E., Gurwell, M., Butler, B., Moullet, A., Moreno, R., Bockelée-Morvan, D., Biver, N., Fouchet, T., Lis, D., Stern, A., Young, L., Young, E., Weaver, H., Boissier, J., Stansberry, J., 2015. Detection of HCN in Pluto's atmosphere, in: American Astronomical Society, DPS Meeting #47, id.105.07.

Levine, S., Gregory, L., Harvey, A., Howell, E., Borucki, J., Orville, E., 1982. Production of Nitric Oxide by Lightning on Venus. Geophys. Res. Lett. 9, 893–896.

Li, C., Zhang, X., Gao, P., Yung, Y., 2015. Vertical Distribution of C3-Hydrocarbons in the Stratosphere of Titan. Astrophys. J. Lett. 803, L19. doi:10.1088/2041-8205/803/2/L19

Li, C., Zhang, X., Kammer, J.A., Liang, M., Shia, R., Yung, Y.L., 2014. A non-monotonic eddy diffusivity profile of Titan's atmosphere revealed by Cassini

observations. Planet. Space Sci. 104, 48–58. doi:10.1016/j.pss.2013.10.009

Lorenz, R.D., Mckay, C.P., Lunine, J.I., 1997. Photochemically Driven Collapse of Titan's Atmosphere. Science (80-.). 275, 642–645.

Lorenz, R.D., Mitchell, K.L., Kirk, R.L., Hayes, A.G., Aharonson, O., Zebker, H.A., Paillou, P., Radebaugh, J., Lunine, J.I., Janssen, M.A., Wall, S.D., Lopes, R.M., Stiles, B., Ostro, S., Mitri, G., Stofan, E.R., 2008. Titan's inventory of organic surface materials. Geophys. Res. Lett. 35, 4–9. doi:10.1029/2007GL032118

Lunine, J.I., Stevenson, D.J., Yung, Y.L., 1983. Ethane Ocean on Titan. Science (80-.). 222, 1229–1230.

Mack, J., Bolton, J.R., 1999. Photochemistry of nitrite and nitrate in aqueous solution: a review. J. Photochem. Photobiol. A Chem. 128, 1–13. doi:10.1016/S1010-6030(99)00155-0

Mancinelli, R.L., McKay, C.P., 1988. The evolution of nitrogen cycling. Orig. life Evol. Biosph. 18, 311–325.

Martin, R.S., Mather, T. a., Pyle, D.M., 2007. Volcanic emissions and the early Earth atmosphere. Geochim. Cosmochim. Acta 71, 3673–3685. doi:10.1016/j.gca.2007.04.035

Martin, W., Baross, J., Kelley, D., Russell, M.J., 2008. Hydrothermal vents and the origin of life. Nat. Rev. Microbiol. 6, 805–814. doi:10.1038/nrmicro1991

McKay, C.P., Pollack, J.B., Courtin, R., 1991. The Greenhouse and Antigreenhouse Effects on Titan. Science (80-.). 253, 1118–1121.

Mielke, R.E., Robinson, K.J., White, L.M., McGlynn, S.E., McEachern, K., Bhartia, R., Kanik, I., Russell, M.J., 2011. Iron-Sulfide-Bearing Chimneys as Potential Catalytic Energy Traps at Life's Emergence. Astrobiology 11, 933–950. doi:10.1089/ast.2011.0667

Milner-white, E.J., Russell, M.J., 2011. Functional Capabilities of the Earliest Peptides and the Emergence of Life. Genes (Basel). 2, 671–688. doi:10.3390/genes2040671

Milner-White, E.J., Russell, M.J., 2008. Predicting the conformations of peptides and proteins in early evolution. A review article submitted to Biology Direct. Biol. Direct 3, 3. doi:10.1186/1745-6150-3-3

Mloszewska, A.M., Pecoits, E., Cates, N.L., Mojzsis, S.J., O'Neil, J., Robbins, L.J., Konhauser, K.O., 2012. The composition of Earth's oldest iron formations: The Nuvvuagittuq Supracrustal Belt (Québec, Canada). Earth Planet. Sci. Lett. 317–318, 331–342. doi:10.1016/j.epsl.2011.11.020

Moses, J.I., Allen, M., Yung, Y.L., 1992. Nucleation and Aerosol Formation Neptune's Atmosphere. Icarus 99, 318–346.

Moses, J.I., Fouchet, T., Be, B., Gladstone, G.R., Lellouch, E., 2005. Photochemistry and diffusion in Jupiter's stratosphere: Constraints from ISO observations and comparisons with other giant planets. J. Geophys. Res. 110, 1–45. doi:10.1029/2005JE002411

Nair, H., Allen, M., Anbar, A.D., Yung, Y.L., Clancy, R.T., 1994a. A Photochemical Model of the Martian Atmosphere. Icarus 111, 124–150. doi:10.1006/icar.1994.1137

Nair, H., Allen, M., Anbar, A.D., Yung, Y.L., Clancy, R.T., 1994b. A Photochemical Model of the Martian Atmosphere. Icarus 111.

Nielsen, S.G., Rehkämper, M., Teagle, D.A.H., Butterfield, D.A., Alt, J.C., Halliday, A.N., 2006. Hydrothermal fluid fluxes calculated from the isotopic mass balance of thallium in the ocean crust. Earth Planet. Sci. Lett. 251, 120–133. doi:10.1016/j.epsl.2006.09.002

Niemann, H.B., Atreya, S.K., Bauer, S.J., Carignan, G.R., Demick, J.E., Frost, R.L., Gautier, D., Paulkovich, M., Raulin, F., Raaen, E., Way, S.H., 2005. The abundances of constituents of Titan's atmosphere from the GCMS instrument on the Huygens probe. Nature 438, 779–784. doi:10.1038/nature04122

Nimmo, F., Hamilton, D.P., McKinnon, W.B., Schenk, P.M., Binzel, R.P., Bierson, C.J., Beyer, R.A., Moore, J.M., Stern, S.A., Weaver, H.A., Olkin, C.B., Young, L.A., Smith, K.E., Team, the N.H.G.G.& I.T., 2016. Reorientation of Sputnik Planitia implies a subsurface ocean on Pluto. Nature 540, 94–96. doi:10.1038/nature20148

Nitschke, W., Mcglynn, S.E., Milner-white, E.J., Russell, M.J., 2013. On the antiquity of metalloenzymes and their substrates in bioenergetics. Biochim. Biophys. Acta 1827, 871–881. doi:10.1016/j.bbabio.2013.02.008

Nitschke, W., Russell, M.J., 2013. Beating the acetyl coenzyme A-pathway to the origin of life. Philos. Trans. R. Soc. Lond. B. Biol. Sci. 368, 20120258. doi:10.1098/rstb.2012.0258

Nna Mvondo, D., Navarro-Gonzalez, R., McKay, C.P., Coll, P., Raulin, F.,

2001. Production of nitrogen oxides by lightning and coronae discharges in simulated early Earth, Venus and Mars environments. Adv. Space Res. 27, 217–23. doi:http://dx.doi.org/10.1016/S0273-1177(01)00050-3

Palmer, M.Y., Cordiner, M.A., Nixon, C.A., Charnley, S.B., Teanby, N.A., Kisiel, Z., Irwin, P.G.J., Mumma, M.J., 2017. ALMA detection and astrobiological potential of vinyl cyanide on Titan. Sci. Adv. 3, 1–7.

Peters, J.W., Miller, A., Jones, A.K., King, P.W., Adams, M.W.W., 2016. Electron bifurcation. Curr. Opin. Chem. Biol. 31, 146–152.

Pierrehumbert, R.T., 2010. Principles of Planetary Climates. Cambridge University Press, Cambridge.

Poppe, A.R., 2015. Interplanetary dust influx to the Pluto – Charon system. Icarus 246, 352–359. doi:10.1016/j.icarus.2013.12.029

Proskurowski, G., Lilley, M.D., Kelley, D.S., Olson, E.J., 2006. Low temperature volatile production at the Lost City Hydrothermal Field, evidence from a hydrogen stable isotope geothermometer. Chem. Geol. 229, 331–343. doi:10.1016/j.chemgeo.2005.11.005

Rannou, P., West, R., 2018. Supersaturation on Pluto and elsewhere. Icarus 312, 36–44. doi:10.1016/j.icarus.2018.04.025

Ribas, I., Guinan, E.F., Güdel, M., Audard, M., 2005. Evolution of the solar activity over time and effects on planeary atmospheres. I. High-energy irradiances (1–1700 Å). Astrophys. J. 622, 680–694.

Robuchon, G., Nimmo, F., 2011. Thermal evolution of Pluto and implications

for surface tectonics and a subsurface ocean. Icarus 216, 426–439. doi:10.1016/j.icarus.2011.08.015

Romps, D.M., Seeley, J.T., Vollaro, D., Molinari, J., 2014. Projected increase in lightning strikes in the United States due to global warming. Science (80-.). 346, 851–854. doi:10.1126/science.1259100

Russell, M.J., Barge, L.M., Bhartia, R., Bocanegra, D., Bracher, P.J., Branscomb, E., Kidd, R., McGlynn, S., Meier, D.H., Nitschke, W., Shibuya, T., Vance, S., White, L., Kanik, I., 2014. The Drive to Life on Wet and Icy Worlds. Astrobiology 14, 308–343. doi:10.1089/ast.2013.1110

Russell, M.J., Hall, A.J., Martin, W., 2010. Serpentinization as a source of energy at the origin of life. Geobiology 8, 355–371. doi:10.1111/j.1472-4669.2010.00249.x

Russell, M.J., Hall, a J., 1997. The emergence of life from iron monosulphide bubbles at a submarine hydrothermal redox and pH front. J. Geol. Soc. London. 154, 377–402. doi:10.1144/gsjgs.154.3.0377

Russell, M.J., Martin, W., 2004. The rocky roots of the acetyl-CoA pathway. Trends Biochem. Sci. 29, 358–363. doi:10.1016/j.tibs.2004.05.007

Sander, S.P., Ravishankara, A.R., Golden, D.M., Kolb, C.E., Kurylo, M.J., Molina, M.J., Moortgat, G.K., Finlayson-Pitts, B.J., 2003. Chemical Kinetics and Photochemical Data for Use in Atmospheric Studies: Evaluation Number 14. JPL Publ. 02-25 14, 1–334. doi:10.1002/kin.550171010

Schoepp-Cothenet, B., van Lis, R., Philippot, P., Magalon, A., Russell, M.J.,

Nitschke, W., 2012. The ineluctable requirement for the trans-iron elements molybdenum and/or tungsten in the origin of life. Sci. Rep. 2, 1–5. doi:10.1038/srep00263

Schumann, U., Huntrieser, H., 2007. The global lightning-induced nitrogen oxides source. Atmos. Chem. Phys. Discuss. 7, 2623–2818. doi:10.5194/acpd-7-2623-2007

Seyfried, W.E., Pester, N.J., Tutolo, B.M., Ding, K., 2015. The Lost City hydrothermal system: Constraints imposed by vent fluid chemistry and reaction path models on subseafloor heat and mass transfer processes. Geochim. Cosmochim. Acta 163, 59–79. doi:10.1016/j.gca.2015.04.040

Shibuya, T., Russell, M.J., Takai, K., 2016. Free energy distribution and hydrothermal mineral precipitation in Hadean submarine alkaline vent systems: Importance of iron redox reactions under anoxic conditions. Geochim. Cosmochim. Acta 175, 1–19. doi:10.1016/j.gca.2015.11.021

Sleep, N.H., Zahnle, K., Neuhoff, P.S., 2001. Initiation of clement surface conditions on the earliest Earth. Proc. Natl. Acad. Sci. U. S. A. 98, 3666–3672. doi:10.1073/pnas.071045698

Smith, E., Morowitz, H.J., 2016. The Origin and Nature of Life on Earth. Cambridge University Press, Cambridge.

Stevenson, J., Lunine, J., Clancy, P., 2015. Membrane alternatives in worlds without oxygen: Creation of an azotosome. Sci. Adv. 1, 1–8.

Strobel, D.F., Zhu, X., 2017. Comparative planetary nitrogen atmospheres: Density and thermal structures of Pluto and Triton. Icarus 291, 55–64.

doi:10.1016/j.icarus.2017.03.013

Summers, D.P., 2005. Ammonia formation by the reduction of nitrite/nitrate by FeS: ammonia formation under acidic conditions. Orig. Life Evol. Biosph. 35, 299–312. doi:10.1007/s11084-005-2040-1

Summers, D.P., Khare, B., 2007. Nitrogen fixation on early Mars and other terrestrial planets: experimental demonstration of abiotic fixation reactions to nitrite and nitrate. Astrobiology 7, 333–341. doi:10.1089/ast.2006.0032

Tobie, G., Choukroun, M., Grasset, O., Le Mouélic, S., Lunine, J.I., Sotin, C., Bourgeois, O., Gautier, D., Hirtzig, M., Lebonnois, S., Le Corre, L., 2009. Evolution of Titan and implications for its hydrocarbon cycle. Philos. Trans. R. Soc. A 367, 617–631. doi:10.1098/rsta.2008.0246

Tobie, G., Lunine, J.I., Sotin, C., 2006. Episodic outgassing as the origin of atmospheric methane on Titan. Nature 440, 61–64. doi:10.1038/nature04497

Trolard, F., Bourrié, G., 2012. Fougerite a natural layered double hydroxide in gley soil: habitus, structure, and some properties. Clay Miner. Nat. - Their Charact. Modif. Appl. 171–188.

Tsang, W., Herron, J.T., 1991. Chemical Kinetic Data Base for Propellant Combustion I. Reactions Involving NO, NO2, HNO, HNO2, HCN and N2O. J. Phys. Chem. Ref. Data 20, 609–663. doi:10.1063/1.555890

White, L.M., Bhartia, R., Stucky, G.D., Kanik, I., Russell, M.J., 2015. Mackinawite and greigite in ancient alkaline hydrothermal chimneys: Identifying potential key catalysts for emergent life. Earth Planet. Sci. Lett.

430, 105–114. doi:10.1016/j.epsl.2015.08.013

Willacy, K., Allen, M., Yung, Y.L., 2016. A new astrobiological model of the atmosphere of Titan. submitted 1–17.

Wilson, E.H., Atreya, S.K., 2009. Titan's Carbon Budget and the Case of the Missing Ethane. J. Phys. Chem. 113, 11221–11226.

Wong, M.L., Fan, S., Gao, P., Liang, M., Shia, R., Yung, Y.L., Kammer, J.A., Summers, M.E., Gladstone, G.R., Young, L.A., Olkin, C.B., Ennico, K., Weaver, H.A., Stern, S.A., 2017. The photochemistry of Pluto's atmosphere as illuminated by New Horizons. Icarus 287, 110–115. doi:10.1016/j.icarus.2016.09.028

Wong, M.L., Yung, Y.L., Gladstone, G.R., 2015. Pluto's implications for a Snowball Titan. Icarus 246, 192–196. doi:10.1016/j.icarus.2014.05.019

Wordsworth, R.D., Forget, F., Selsis, F., Millour, E., Charnay, B., Madeleine, J.-B., 2011. Gliese 581D Is the First Discovered Terrestrial-Mass Exoplanet in the Habitable Zone. Astrophys. J. 733, L48. doi:10.1088/2041-8205/733/2/L48

Yung, Y.L., Allen, M., Pinto, J.P., 1984. Photochemistry of the Atmosphere of Titan: Comparison Between Model and Observations. Astrophys. J. Suppl. Ser. 55, 465–506.

Yung, Y.L., DeMore, W.B., 1999. Photochemistry of Planetary Atmospheres. Oxford.

Zhang, X., Strobel, D.F., Imanaka, H., 2017. Haze heats Pluto's atmosphere yet explains its cold temperature. Nature 551, 352–355.

doi:10.1038/nature24465

Zhu, X., Strobel, D.F., Erwin, J.T., 2014. The density and thermal structure of Pluto' s atmosphere and associated escape processes and rates. Icarus 228, 301–314. doi:10.1016/j.icarus.2013.10.011